Title: Vitamin D constrains inflammation by modulating the expression of key genes on Chr17q12-21.1

Authors: Ayşe Kılıç[1*], Arda Halu[1*#], Margherita De Marzio[1,2], Enrico Maiorino[1], Melody G. Duvall[3], Thayse Brueggemann[3], Joselyn J. Rojas Quintero[3], Robert Chase[1], Hooman Mirzakhani[1], Ayse Özge Sungur[4, 5], Janine Koepke[5], Taiji Nakano[6], Hong Yong Peh[3], Nandini Krishnamoorthy[3], Raja-Elie Abdulnour[3], Katia Georgopoulos[7], Augusto A. Litonjua[8], Marie B. Demay[9], Harald Renz[10,11], Bruce D. Levy[3] and Scott. T Weiss[1*#]

Affiliations:

[1] Channing Division of Network Medicine, Department of Medicine, Brigham and Women's Hospital and Harvard Medical School; Boston, MA, USA.

[2] Department of Environmental Health, Harvard TH Chan School of Public Health; Boston, MA, USA.

[3] Division of Pulmonary and Critical Care Medicine, Department of Medicine, Brigham and Women's Hospital and Harvard Medical School; Boston, MA, USA.

[4] Behavioral Neuroscience, Experimental and Biological Psychology, Philipps-University Marburg; Marburg, Germany.

[5] Excellence Cluster Cardio-Pulmonary System (ECCPS), Justus Liebig University Giessen; Giessen, Germany.

[6] Department of Pediatrics, Graduate School of Medicine, Chiba University; Chiba, Japan.

21 [7] Cutaneous Biology Research Center, Massachusetts General Hospital and Harvard Medical
22 School; Charlestown, Massachusetts, USA.

23 [8] Division of Pediatric Pulmonary Medicine, Golisano Children's Hospital at Strong, University
24 of Rochester Medical Center; Rochester, NY, USA.

25 [9] Endocrine Unit, Massachusetts General Hospital and Harvard Medical School; Boston, MA,
26 USA.

27 [10] Institute of Laboratory Medicine and Pathobiochemistry, Molecular Diagnostics, Philipps
28 University of Marburg and German Center for Lung Research (DZL); Marburg, Germany.

29 [11] Department of Clinical Immunology and Allergology, Laboratory of Immunopathology
30 Sechenov University; Moscow, Russia.

31 *These authors contributed equally to the manuscript.

32 #Corresponding author. Arda Halu (rehal@channing.harvard.edu), Scott Weiss
33 (restw@channing.harvard.edu)

34

35

36

37

38 **Abstract:** Vitamin D possesses immunomodulatory functions and vitamin D deficiency has been
39 associated with the rise in chronic inflammatory diseases, including asthma (1). Vitamin D
40 supplementation studies do not provide insight into the molecular genetic mechanisms of vitamin
41 D mediated immunoregulation. Here we provide evidence for vitamin D regulation of two human

chromosomal loci, Chr17q12-21.1 and Chr17q21.2, reliably associated with autoimmune and chronic inflammatory diseases (2–4). We demonstrate increased vitamin D receptor (VDR) expression in mouse lung CD4+ Th2 cells, differential expression of Chr17q12-21.1 and Chr17q21.2 genes in Th2 cells based on vitamin D status and identify the IL-2/Stat5 pathway as a target of vitamin D signaling. Vitamin D deficiency caused severe lung inflammation after allergen challenge in mice that was prevented by long term prenatal vitamin D supplementation. Mechanistically, vitamin D induced the expression of the *Ikzf3* encoded protein Aiolos to suppress IL-2- signaling and ameliorate cytokine production in Th2 cells. These translational findings demonstrate mechanisms for the immune protective effect of vitamin D in allergic lung inflammation with a strong molecular genetic link to the regulation of both Chr17q12-21.1 and Chr17q21.2 genes and suggest further functional studies and interventional strategies for long-term prevention of asthma and other autoimmune disorders.

One Sentence Summary: Vitamin D regulates two human chromosomal loci, Chr17q12-21.1 and Chr17q21.2, that are associated with autoimmune and chronic inflammatory diseases.

INTRODUCTION

The vitamin D receptor was genetically associated with asthma in 2004 (5) and high intake of vitamin D by pregnant women is associated with about a 50% reduction in asthma risk in the mother's offspring (6, 7). Together, these exciting findings led to a comprehensive theory about how vitamin D deficiency could influence asthma occurrence through its effects on lung and immune system development and that progressive decreases in vitamin D intake from 1946 onward could be contributing to the epidemic of allergic and autoimmune diseases (1). Vitamin D

64 deficiency is the most common vitamin deficiency in the world today and is particularly prevalent
65 in pregnant women where the fetal lung and immune system are developing (8–10).

66 To determine the impact of vitamin D supplementation, we performed a clinical trial, the Vitamin
67 D Antenatal Asthma Trial (VDAART) in pregnant women who either had allergies or asthma or
68 had family members with these conditions. The participants were given either 4400 IU of vitamin
69 D3 or 400 IU and were followed throughout their pregnancy and for the first six years of the life
70 of the child (11). The results of the trial were not statistically significant using conventional intent
71 to treat analysis (12, 13) but the reasons were complex, as is often seen when the effects of nutrients
72 are studied. Most importantly, unlike conventional drug trials where one compares drug to no drug
73 or alternative drug, in nutrient trials there is nutrient already present in the placebo group. This
74 creates misclassification that can reduce trial power. When we performed a meta-analysis of the
75 two pregnancy related trials of vitamin D, we got a statistically significant reduction in asthma in
76 the offspring of women who had the higher vitamin D intake during pregnancy and, when we
77 adjusted for the baseline level of vitamin D in the meta-analysis, we got a reduction in asthma risk
78 of 50 percent, exactly what we saw in the observational studies performed previously (14, 15).

79 To link the results of the VDAART trial directly to the chr17q12 locus we genotyped SNP,
80 rs12936231, in ZPBP2, the gene adjacent to ORMDL3, and stratified the VDAART trial results
81 by maternal genotype at this locus and found that the vitamin D effect in the trial was significantly
82 influenced by genotype with the GG genotype exhibiting a protective effect on asthma risk in the
83 child and the CC or GC genotype not being responsive to vitamin D, additionally this result was
84 related to sphingolipid production with the children protected from asthma having higher
85 sphingolipid production (3).

86 This SNP (rs12936231) is one of two SNPs (the other being rs4065275) that alter the chromatin
87 state of a regulatory domain, specifically two CTCF binding sites, in the chr17q12-21.1 locus that
88 are correlated with the expression of ORMDL3 (16, 4). 4C-seq assays previously demonstrated
89 that the ORMDL3 promoter interacts with a long-range enhancer in IKZF3 that promotes (or
90 represses) transcription of ORMDL3 in cells expressing both genes and the binding of CTCF per
91 the G allele of rs12936231 in ZPBP2 blocks this interaction resulting in reduced transcription of
92 ORMDL3 on haplotypes with the rs12936231-G allele (4). If rs12936231 is not activated then
93 there is activation of the other CTCF binding site (rs4065275) intronic to ORMDL3 thus favoring
94 the expression of ORMDL3 and increased asthma risk (4).

95 Mouse models have contributed to our understanding of ORMDL3 function as mice expressing
96 the ORMDL3 transgene exhibit spontaneous increases in airway hyper responsiveness, the
97 essential feature of asthma. This increase in AHR was associated with airway remodeling and peri
98 bronchial fibrosis without airway inflammation (17). ORMDL3 is pleotropic, influencing Ca++
99 signaling, and the unfolded protein response. Most importantly, increased expression of ORMDL3
100 inhibits the enzyme serine palmityl-transferase, the rate limiting step in the production of
101 sphingolipids and ORMDL3 TG mice have reduced levels of sphingolipids (18). What has been
102 unclear is how ORMDL3 is controlled.

103 In the current manuscript we provide evidence for vitamin D regulation of two human
104 chromosomal loci, Chr17q12-21.1 and Chr17q21.2, reliably associated with autoimmune and
105 chronic inflammatory diseases. We demonstrate increased vitamin D receptor (VDR) expression
106 in mouse lung CD4+ Th2 cells, differential expression of these Chr17q12-21.1 and Chr17q21.2
107 genes in Th2 cells based on vitamin D status and identify the IL-2/Stat5 pathway as a target of
108 vitamin D signaling. Vitamin D induced the expression of the *Ikzf3* encoded protein Aiolos to

109 suppress IL-2- signaling and ameliorate cytokine production in Th2 cells thus demonstrating a
110 mechanism for how vitamin D influences autoimmunity.

111

112 **MATERIALS AND METHODS**

113 ***In silico analysis of VDR binding sites on Chr17q12-21***

114 For our *in-silico* analysis, we focused on two genomic regions that are known to harbor variants
115 associated with asthma and autoimmune disease susceptibility. The first one is a 240 kb region
116 that covers parts of the 17q12 and 17q21.1 loci and contains IKZF3, ZPBP2, ORMDL3, GSDMA
117 and GSDMB (chr17: 37,899,254–38,139,253; hg19) and the second one is a 420 kb region in the
118 17q21.2 locus that includes STAT3, STAT5A and STAT5B (chr17: 40,330,000-40,750,000;
119 hg19). When selecting these genomic ranges, our criterion was to make the window inclusive of
120 any potential enhancer regions targeting the above genes of interest. We used the GeneHancer (19)
121 track in the UCSC Genome Browser (http://genome.ucsc.edu) to determine predicted enhancer-
122 target gene interactions. We obtained VDR, IKZF3, CTCF and Vitamin D-sensitive CTCF binding
123 sites from (20–23), converted their genomic coordinates to hg19 if a different genome build was
124 used in the original publication, and added them as custom tracks on the Genome Browser. We
125 retrieved the known disease and trait associations in these loci from the NHGRI-EBI GWAS
126 Catalog (downloaded on 7/26/2021) (24) and retained all hits that were deemed significant ($p<10^{-}$
127 ^{5}). We downloaded significant single-tissue eQTLs for IKZF3 and PSMCIP3 in all tissues from
128 the Common Fund (CF) Genotype-Tissue Expression Project (GTEx) Analysis Release V8
129 (dbGaP Accession phs000424.v8.p2), through the GTEx Portal
130 (https://www.gtexportal.org/home/) in July 2021. We calculated linkage disequilibrium (LD)

131 using the NCI LDmatrix Tool (https://ldlink.nci.nih.gov/?tab=ldmatrix), and by selecting all
132 available populations.

133 ***Gene expression analysis in VDAART cohort***

134 To understand the putative mechanism linking IKZF3 expression and Vitamin D to asthma risk
135 we considered umbilical cord blood (CB) RNA-seq data from the VDAART trial. Total RNA was
136 isolated from cord blood using the QIAGEN PAXgene Blood RNA Kit (Qiagen) according to the
137 manufacturer's protocol. Quality was assessed using the Nanodrop 8000 spectrophotometer
138 (ThermoFisher Scientific). Sequencing libraries were constructed with the TruSeq® Stranded
139 Total RNA Library Prep Globin Kit (Illumina) and the NEXTflex Small RNA sequencing Kit v3
140 (Boo Scientific). Sequencing was performed using a NextSeq 550 instrument (Illumina). Trimmed
141 reads were mapped to The GRCh38 reference genome using STAR (25). Read counts were
142 computed with htseq (26). The data includes 443 expression profiles of pregnant women with and
143 without asthma undergoing measurements of Vitamin D levels in their CB. Each sample is
144 matched with the observed patterns of wheezing and asthma in the newborn. We filtered all the
145 samples where information about Vitamin D levels, asthma/wheezing patterns or other covariates
146 were missing, obtaining 393 expression profiles. Data was normalized with the voom function of
147 the edgeR R package (27), and Vitamin D levels were binarized using 30 ng/ml as threshold. We
148 performed logistic regression of asthma status as a function of the expression levels of IKZF1 and
149 IKZF3, including their interaction term and the interaction between IKZF3 and Vitamin D. Since
150 IKZF3 forms homodimers and heterodimers with IKZF1, we included IKZF1 in the model. We
151 adjusted the model for maternal asthma status and child race.

152 ***Mice***

153 All animal studies were approved by the institutional animal care committee. Mice were
154 maintained in a virus- and parasite-free animal facility under a 12-h light, 12-h dark cycle.
155 C57BL6/J wild type (WT) mice were bred and housed at the MGH animal facility. Vitamin D-
156 deficient mice (C57BL6/J) were bred and maintained in a UV-free environment and weaned onto
157 a similar diet lacking vitamin D metabolites (TD97340; Harlan Teklad) that results in undetectable
158 circulating 25-hydroxyvitamin D levels (28). $VDR^{-/-}$ mice ($Vd^{rtm1Mbd/J}$), on C57BL6/J background,
159 were bred and housed at the MGH animal facility, weaned at 18 d on a diet that maintains normal
160 mineral ion homeostasis in the absence of VDR signaling (2% calcium, 1.25% phosphorus, 20%
161 lactose supplemented diet, TD96348; Harlan Teklad, Madison WI) (29). BALB/c male and female
162 mice were purchased from Charles River Laboratories at 6–8 weeks of age and fed with diets
163 supplemented with varying amounts of vitamin-D3 (TD97340 was used as base diet and
164 supplemented with either 400 IU vitamin D/kg, 1000 IU vitamin D/kg or 4000 IU vitamin D/kg).
165 Mice were bred on the specific diets for two generations to assure stabilization of vitamin D levels.
166 Resulting F2 litters were used for the experiments. Mice were housed under standard conditions
167 with free access to rodent chow and water. All animal experiments were carried out in accordance
168 with NIH Guidelines for the Care and Use of Laboratory Animals as well as guidelines prescribed
169 by the Institutional Animal Care and Use Committee (IACUC) at Brigham and Women's Hospital
170 (2016N000357), Massachusetts General Hospital (2004N000113) and Harvard Medical Area
171 (05115) (AAALAC 1729).

172 ***House dust mite induced-airway inflammation***

173 Mice were exposed to D. pteronyssinus extracts (Greer Laboratories, 10.52 EU/mg endotoxin) via
174 the intranasal application of HDM (25 μg in saline) on days 1,2,3, 8 to 15. Control mice received

175 equal volumes of saline (Hospira Inc., Lake Forest, IL, USA). Twenty-four hours after the final
176 challenge, mice were sacrificed, and specimens sampled.

177 ***Bronchoalveolar Lavage***

178 Bronchoalveolar Lavage (BAL) was performed with 2 × 1 mL of PBS/0.02% bovine serum
179 albumin (BSA). The total number of leukocytes was determined using a TC20 Automated Cell
180 Counter (BioRad Systems). To differentiate cell types, cytospins were prepared and stained with
181 Kwik-Diff solutions as per manufacturer's instructions (Fisher Scientific) and 200 immune cells
182 per slide were counted.

183 ***Histological staining***

184 Lungs were perfusion fixed with zinc fixative (BD Pharmingen, San Diego, CA) Tissues were
185 paraffin embedded, divided into sections, and stained with hematoxylin and eosin by MGH
186 DF/HCC Specialized Histopathology Services Core Histology Core. After paraffin embedment, 3-
187 μm sections were stained with hematoxylin and eosin.

188 ***Measurements of serum immunoglobulins***

189 Blood samples were collected 24 hours after the final aerosol challenge and serum was prepared.
190 Total IgE levels were measured by ELISA (Chondrex) according to manufacturer's instructions.

191 ***Dissociation of mouse tissues, in vitro polarization of CD4 Th-subsets and flow cytometry***
192 ***analyses***

193 Lungs were perfused via the right heart ventricle with PBS, excised, and digested with collagenase
194 D (2 mg/ml; Roche) in RPM 1640 (Sigma-Aldrich) for 30 minutes at 37°C. The cell suspension
195 was washed twice with PBS. Erythrocytes were removed by hypotonic lysis. Cells were washed
196 twice with PBS and sieved with 30-μm cell strainers (Miltenyi Biotec). The resulting single cells

197 suspension was used to detect leukocyte populations (CD45 BV421 [clone: 104; Biolegend], CD4
198 PerCPeFluor710 [RM4-5; eBioscience], CD8a APC-Cy7 [53-6.7; Biolegend], CD19 PE-Cy7
199 [6D5; Biolegend]) and CD4+ Foxp3+ Treg (CD45 BV421, CD4 PerCPeFluor710, Foxp3 PE [FJK-
200 16s; Thermo Fisher]), VDR AlexaFluor647 (D2K6W; Cell Signaling Technologies), Aiolos PE
201 (8B2; Biolegend) and cytokine production by Th-cells (see below). Spleens were excised and
202 mononuclear cells were isolated using a syringe plunger and 100-µm cell strainers. Red blood cells
203 were removed by hypotonic lysis. Tonicity was restored by the addition of RPMI 1640 (Sigma
204 Aldrich). The resulting cell suspension was washed twice with PBS and used for the isolation of
205 naïve CD4+ T cells according to the manufacturer's instructions (Naive T Cell Isolation Kit II;
206 Miltenyi Biotec). Naive CD4+ T cell purity was assessed by staining for CD4 PerCPeFluor710
207 (clone: RM4-5), CD44 FITC (IM7), and CD62L PE (mel-14). Naïve T cells were activated with
208 plate bound anti-CD3ε (5 µg/ml, clone: 145-2C11, BD Biosciences) and soluble anti-CD28 (0.5
209 µg/ml, clone: 37.51, BD Biosciences). Th-subset polarization was induced by exposing naïve
210 CD4+Tcells to following culture conditions for 3 days. Th1 cells: recombinant murine IL-12
211 (rmIL-12) (10 ng/mL; Peprotech), anti–IL-4 (5 µg/mL; BD Biosciences); Th2 cells: rmIL-4 (20
212 ng/mL; Peprotech), anti–IFN-γ (5 µg/mL; BD Biosciences), and anti–IL-12 (5 µg/mL; BD
213 Biosciences); Treg: rmTGFβ1 (2 ng/mL; Peprotech), anti–IL-4 (5 µg/mL), anti–IFN-γ (5 µg/mL)
214 for 3 days. Proliferation of Th1 and Th2 cells was induced using rmIL-2 (20 ng/mL; Peprotech) in
215 the presence of Th-polarizing reagents for an additional 2 days. Polarization efficiency was
216 verified by staining for intracellular cytokines (please see below) or Foxp3 expression (see above).

217 For intracellular cytokine staining, cells were stimulated with phorbol 12-myristate 13-acetate
218 (PMA)/ionomycin and brefeldin A (Cell Stimulation Cocktail; Tonbo Biosiences) for 4 hours.
219 Cells were fixed with Fixation Buffer (Biolegend). Cells were permeabilized using 0.3% saponin

220 in FACS buffer (0.5% FBS in PBS). Antibody staining was performed for 30 minutes in the dark
221 using CD4, IFN-γ (XMG1.2-FITC), IL-10 (JES5-16E3-PE), IL-13 (eBio13A-eFluor660), IL-17A
222 (TC11-18H10.1-PE-Cy7). Cells were washed twice with permeabilization buffer and suspended
223 in FACS buffer. For analysis, 30,000 counts (in the CD4+ gate) were recorded on a FACSFortessa
224 (BD Biosciences) and analyzed with FlowJo software (v10; Tree Star).

225 ***Western blot analyses***

226 Cells were lysed in 50 mmol/L Tris/HCl (pH 7.5), 150 mmol/L NaCl, 1% NP-40, and 1× protease
227 and phosphatase inhibitor mix (both Roche) for 15 minutes on ice. Lysates were clarified, and total
228 protein concentrations were measured with BCA (Pierce). Proteins (20 µg) were separated on
229 gradient gels (Mini-PROTEAN® TGX; BioRad) and transferred on a Immun-Blot PVDF
230 membrane (BioRad). Unspecific binding was blocked using 5 % milk powder in TBST for 30 min.
231 Anti-VDR (D2K6W, 1:1000; Cell Signaling Technologies, CST) was incubated in 0.5 % milk
232 powder in TBST overnight at 4° C. Membranes were washed 3 times with TBST and incubated
233 with secondary anti-rabbit IgG, HRP-linked Antibody (#7074; CST) for 2 hours. To control for
234 equal loading, membranes was probed for β-actin (AC-15; 1:10,000; Sigma-Aldrich) expression
235 for 2 hrs. at RT. Protein bands were visualized with Luminol reagent (Pierce) using the ChemiDoc
236 XRS+system (BioRad).

237 ***Immunofluorescence staining for confocal microscopy***

238 *In vitro* polarized Th2 cells (see above) were stimulated with 100 nm calcitriol (in ethanol) or
239 ethanol [equal v/v] for the final 24 hrs of culture. Cells were washed twice with PBS and spun onto
240 poly-L-lysine coated glass slides. After drying, cells were fixed with 4 % PFA in PBS for 15 min.
241 Cells were permeabilized using 0.2% Triton X-100 in PBS for 20 min. Cells were washed 3 times
242 for 5 min with PBS and incubated with Image-iT FX Signal Enhancer (Thermo Fisher Scientific)

243 for 30 min at RT. After three consecutive washes with PBS, unspecific binding was blocked using
244 blocking buffer (PBS/5 % goat serum/0.3 % Triton X-100) for 60 min at RT. Primary antibodies
245 directed against CD4-FITC (clone; 1:100, BD Biosciences), VDR (D2K6W; 1: 200, CST) were
246 incubated in a humidified chamber over night at 4° C. After 3 washes with PBS, slides were
247 incubated with the secondary reagent, anti-rabbit-Cy3 (1:500; Thermo) for 30 min at RT in the
248 dark. After three more washes with PBS, slides were mounted with ProLong Gold with DAPI
249 according to manufacturer's instructions (Invitrogen). Images were acquired in a single z-plane
250 using a Zeiss immunofluorescence microscope with a 40x objective.

251 ***Total RNA isolation, quality control, and RNA-sequencing analysis***

252 Total RNA was isolated using TRIzol™ Reagent (Invitrogen) according to the manufacturer's
253 instructions. Quality was assessed using the Nanodrop 8000 spectrophotometer. Sequencing
254 libraries were constructed with the TruSeq® Stranded Total RNA Library Prep Globin Kit
255 (Illumina). Sequencing was performed using a HiSeq. 2500 instrument (Illumina). Trimmed reads
256 were mapped to the GRCm38 reference genome using STAR (25). Read counts were computed
257 with htseq (26). Data were normalized and differential expression was analyzed with the R package
258 DESeq2 (v.1.34.0) (30) using a false discovery rate (FDR) < 0.05.

259 ***Pathway enrichment, Overrepresentation and Gene Set Enrichment analysis***

260 KEGG pathway, overrepresentation and gene set enrichment analyses were performed with the
261 "enrichKEGG", "enrichr" and "GSEA" function in the R package "clusterProfiler" (v.3.10.1) with
262 default settings (31). P-values were adjusted using the BH-FDR correction and enriched terms with
263 a p-adj.<0.05 selected.

264 ***Network analysis***

265 RNA-Sequencing data extracted from murine Th2 cells were analyzed using the R package
266 DESeq2 (v.1.22.2) (30). Raw counts were normalized and transformed for variance stabilization
267 using the DESeq2 function rlog (regularized-logarithm transformation). Batch effects were
268 removed using the function removeBatchEffect of the R package LIMMA (32). Gene with counts
269 lower than 5 in at least one sample were removed for downstream analyses. Differential expression
270 analysis was performed between control Th2 cells versus calcitriol stimulated Th2 cells using
271 DeSeq2 (30). The design matrix was built to consider batch effects derived from the RNA isolation
272 process. DESeq2-independent filtering was applied (30) and P values were corrected for multiple
273 hypothesis testing by using the Benjamini-Hochberg (BH)-FDR adjustment (33).

274 The PPI network used in our network analysis was developed by Silverbush et al. (34). As
275 described in the original paper, this human PPI network was reconstructed by integrating large
276 scale PPI databases, drug response repositories, and cancer genomics data. Only the largest
277 connected component of the network was considered, resulting in an interactome of 15,500
278 proteins and 234,585 consensus-oriented interactions. Conversion between murine and human
279 gene IDs was performed using the BioMart conversion tool (35). We also assumed a one-to-one
280 correspondence between genes and their protein products in the entire analysis.

281 To identify the active signaling paths in control and calcitriol stimulated Th2 cells, we modelled
282 the transmission of the molecular signal as a sequential path on the PPI network (called a network
283 path) that starts from a receptor, connects the receptor to multiple intermediate proteins, and leads
284 to a transcription factor. Receptors and transcription factors were selected from a predefined list
285 based on their role in Th2 cell biology and IL-2 expression (**Figure 4-table supplement 1**). CD3,
286 CD28, IL-4R, IL-13R were selected based on their role in Th2 differentiation. The IL-2R complex
287 was included due to being a target of vitamin D signaling. TGFβRs were selected based on the

288 immunomodulatory activity of this signaling path in CD4+ T cells. role in mediating
289 immunoregulation. Using this subset of receptors and transcription factors as input for the
290 implementation of our network analysis, we computed all the shortest paths connecting each
291 receptor-transcription factor pair on the PPI network. For both control and calcitriol stimulated
292 Th2 cells, we ranked each network path based on the average expression of the path's nodes. The
293 top selected paths represent the most active downstream processes in Th2 cells in each condition.

294 ***mRNA isolation, reverse transcription, and real-time RT-PCR***

295 Total RNA from in vitro polarized Th2 cells was isolated with the RNeasy Mini Kit (Qiagen).
296 First-strand cDNA synthesis was performed with the Omniscript kit (Qiagen). Quantitative real-
297 time PCR was performed with the SsoFast EvaGreen Supermix Kit (BioRad) on a AriaMx Real-
298 time PCR System (Agilent) as per manufacturer's instructions. Primers sequences used in this
299 study are: Gsdma (sense: 5'-TGC TGT CAA AGG ACG CTA TG-3'; antisense: 5'-TCA ACC
300 AGC TTC AGT TGC AC-3'), IL-2 (sense: 5'-CCC ACT TCA AGC TCC ACT TC-3'; antisense:
301 5'-ATC CTG GGG AGT TTC AGG TT-3'), Ikfz3 (5'-TGT CAC CTC TGC AAC TAC GC-3'; 5'-
302 TTC CGC AGA ACT CAC ACT TG-3'), Ormdl3 (sense: 5'-CAC ACG GGT GAT GAA C AG
303 TC-3'; antisense: 5'-CTT TGC CTT GGT CTG GAG TC-3'), Stat3 (sense: 5'-GAG GAG CTG
304 CAG CAG AAA GT-3'; antisense: 5'-TCG TGG TAA ACT GGA CAC CA-3'), Stat5a (sense: 5'-
305 TAC ATG GAC CAG GCT CCT TC-3'; antisense: 5'-GTC AAA CTC GCC ATC TTG GT-3'),
306 Stat5b (sense: 5'-TGT GGA TAC AGG CTC AGC AG-3'; antisense: 5'-TGG GTG GCC TTA
307 ATG TTC TC-3'). Relative gene expression levels were calculated with the $2^{-\Delta\Delta Ct}$ method, with
308 normalization to the murine ribosomal L32 as the housekeeping gene. Data are presented as fold
309 induction over the respective control groups (vehicle or WT). All standard procedures were
310 performed according to the manufacturer's instructions.

311 ***Quantification and statistical analysis***

312 For each figure the number of replicates per experiment is indicated in the corresponding figure
313 legend. In the figures, mean and standard error of the mean (s.e.m.) are presented and error bars
314 represent the mean ± s.e.m. Two group comparisons were analyzed using unpaired two-tailed
315 Student's t-tests (parametric data) and Mann–Whitney U-test (non-parametric data). Multiple
316 group comparisons were analyzed with Kruskal-Wallis and One-way ANOVA test with Tukey's
317 post hoc analysis. *In vivo* experiments were analyzed using Mixed-effect analysis or Two-way
318 ANOVA test with Holm-Šidák's post-hoc analysis (factors: genotype & exposure, diet &
319 exposure). Prism 9.2 (GraphPad Software) was used to calculate statistics. P values of less than
320 0.05 were considered statistically significant.

321

322 **RESULTS**

323 To address the genetic and molecular mechanisms by which vitamin D can influence asthma,
324 allergic and autoimmune disease risk, we studied the genetic loci of two chromosome regions of
325 interest: 1) the 17q12-21.1 region, that includes the well-known asthma-associated *ORMDL3* gene
326 (36), and 2) the 17q21.2 region, that includes the *STAT5* gene, known to be extensively associated
327 with autoimmune diseases (37, 38). We first examined the entire set of significant disease and trait
328 associations in the Chr17q12-21.1 (181 associations) and Chr17q21.2 (100 associations) loci using
329 the NHGRI-EBI GWAS Catalog (24). Both regions had multiple Th1 and Th2 diseases
330 associations with at least one significant SNP. Chr17q12-21.1 had the highest number of
331 associations related to Th2 diseases (**Figure 1*A***) and 17q21.2 had the highest number of
332 associations related to Th1 diseases (**Figure 1-figure supplement 1*A***). To address the possible
333 link to vitamin D intake, we next investigated a potential overlap of these SNPs with VDR binding

334 sites. Out of the 169 VDR binding sites on Chr17, seven were located in the 17q12-21.1 locus,
335 concentrated in two bands on or near *IKZF3* and *ZPBP2* (**Figure 1*B***). These VDR binding sites
336 also overlapped with RXRA binding sites (**Figure 1*B***). To assess their functional relevance, we
337 searched for eQTLs in these VDR binding regions. We found that four cis-eQTLs control *IKZF3*
338 expression in whole blood and EBV-transformed lymphocytes: rs2941522 and rs12946510 in the
339 enhancer region targeting *ORMDL3* and *IKZF3*, and rs1453559 and rs35564481 in the enhancer
340 region targeting *ORMDL3*, *GSDMA* and *GSDMB* (**Figure 1*B***). Rs1453559 and rs2941522 have
341 previous GWAS associations with both asthma and autoimmune diseases (39–41), rs12946510 has
342 previous GWAS associations with autoimmune diseases (42, 43), and rs35564481 has no known
343 GWAS associations. For the 17q21.2 locus, the only VDR binding site resides near the gene
344 *PSMC3IP* in an enhancer site targeting *STAT5A* (**Figure 1-figure supplement 1*B***). PSMC3IP
345 expression is controlled by three eQTLs overlapping with this VDR binding site (rs4793244,
346 rs62078362 and rs111708606), none of which have any known disease associations. These results
347 suggest that vitamin D binding is critical in this genomic region.

348 We next examined the linkage disequilibrium (LD) pattern between the Th1/Th2-associated SNPs
349 and the SNPs in the VDR binding sites (**Figure 1*C***). Out of the seven SNPs with VDR binding
350 sites identified in 17q12-21.1 and 17q21.2, the first four in 17q12-21.1 (rs2941522, rs12946510,
351 rs35564481, rs1453559) were in a high-LD block with many other Th1-Th2 associated SNPs in
352 the same region. These same four SNPs in 17q12-21.1 were also in high-LD with two SNPs in
353 *ZPBP2* and *ORMDL3* (rs12936231 and rs4065275, respectively) that were previously shown to be
354 functionally relevant to asthma (3, 4, 16). Additionally, two of the three SNPs with VDR binding
355 sites in 17q21.2 (rs4793244 and rs62078362) were in strong-LD with three other Th1-Th2
356 associated SNPs in the17q21.2 region (rs11871801, rs2006141, rs4793090). Overall, these results

357 highlight strong statistical association between vitamin D binding sites and multiple genotypic
358 variations linked to asthma, autoimmune and allergic diseases.

359 Two SNPs in *ZPBP2* and *ORMDL3* (rs12936231 and rs4065275, respectively) that were
360 previously shown to be functionally relevant to asthma (3, 4, 16), were also in high linkage
361 disequilibrium with the four SNPs that we identified in the VDR binding regions of the 17q12-
362 21.1 loci (**Figure 1*C***). Importantly, in both the 17q12-21.1 and 17q21.2 regions, the VDR binding
363 sites coincide with CTCF and IKZF3 binding sites, as well as H3K27ac peaks indicating active
364 enhancer sites (**Figure 1*B*, Figure 1-figure supplement 1*B***). In particular, the two enhancer sites
365 in 17q12-21.1 (GH17J039753 and GH17J039859) were both predicted to interact with the
366 *ORMDL3* promoter region (**Figure 1*B***), and the enhancer site in 17q21.2 (GH17J042576) was
367 predicted to interact with the *STAT5A* promoter region (**Figure 1-figure supplement 1*B***). This
368 suggests a similar mechanism to the one described in (4), whereby SNPs in LD with each other in
369 these enhancer sites affect VDR and CTCF binding, the co-dependence of which in turn could
370 modulate *ORMDL3* and *STAT5A* expression. Although it has been shown that CTCF binding sites
371 can be vitamin D-sensitive (7), no such sites were found in our genomic regions of interest (**Figure
372 1*B*, Figure 1-figure supplement 1*B***).

373 Next, we investigated cord blood gene expression data in the Vitamin D Antenatal Asthma
374 Reduction Trial (VDAART) (see Methods) and looked at the genes of interest in the 17q12 and
375 17q21 regions and their interaction with cord blood vitamin D levels as predictors of
376 asthma/wheeze risk at age 3 year of age. After adjusting for relevant covariates (see Methods), the
377 baseline expression term of *IKZF3* was not found to be significantly associated with asthma risk,
378 while the interaction between vitamin D and *IKZF3* was statistically significant (p-val. < 0.05),

379 suggesting that the association of *IKZF3* expression with asthma risk was mediated by vitamin D
380 levels in the cord blood (**Figure 1- table supplement 1**).

381 Based on our bioinformatic analysis of the Chr17q12 and 17q21 regions, we hypothesize that low
382 vitamin D tissue levels is associated with decreased *IKFZ3* expression and increased expression
383 of *ORMDL3*, *STAT3*, *STAT5A*, *STAT5B*, and *IL2*.

384 **Vitamin-D receptor (VDR) is expressed in Th2 cells in allergic airway inflammation**

385 To test our hypothesis of vitamin D activity at the Chr17q12-21 locus we utilized a mouse model
386 of allergic airway inflammation and identified vitamin D responsive leukocyte subsets in house
387 dust mite (HDM)-sensitized and challenged mice using flow cytometry (**Figure 2*A***, **Figure 2-**
388 **figure supplement 2*A-C***). VDR expression was significantly induced in HDM sensitized and
389 challenged mice and almost absent in leukocytes isolated from control (vehicle) lungs (**Figure 2-**
390 **figure supplement 2*C***) but. Within the CD45+ population, VDR expression was high in CD4+ T
391 cells (p= 0.0357), while only very few CD8+ T cells and CD19+ B cells expressed VDR (**Figure**
392 **2*B***, **Figure 2-figure supplement 1*C* HDM**). Within the CD4+ T cell population, highest VDR
393 expression was detected in Gata3+ Th2 cells (p= 0.002 vs Tbet+ and p< 0.0001 vs Foxp3+ T cells).
394 VDR expression was very low in Tbet+ Th1 and CD4+ Foxp3+ Treg cells (Fig. 2b). The
395 differential expression of VDR in Th2 cells was further validated by western blot analysis using
396 naïve CD4+ T cells immediately after isolation (0hrs), after activation with CD3/CD28 for 48 hrs
397 and in *in vitro* polarized Th1, Th2 and iTreg cells with well-defined culture conditions (**Figure 2-**
398 **figure supplement 2*A***, see Methods section). VDR expression appeared as early as day 1 of Th2
399 culture conditions and gradually increased during the polarization process (**Figure 2-figure**
400 **supplement 2*B***). In the absence of the VDR ligand vitamin D, VDR expression localized to the
401 cytoplasm of Th2 cells. Addition of the VDR ligand calcitriol led to a strong translocation of VDR

402 into the nucleus, suggesting functionality of the expressed receptor in the presence of its ligand
403 (**Figure 2-figure supplement 2*C***). These results identify Th2 cells as vitamin D targets in allergic
404 airway inflammation.

405

406 **Vitamin D status regulates the expression of key genes on Chromosome17q12-21.1 and**
407 **Chr17q21.2**

408 Taking cell type specific gene expression and selective expression of VDR in Th2 cells into
409 account, we next analyzed the expression of genes encoded on Chr17q12-21.1 and 17q21.2 loci in
410 WT and vitamin D deficient Th2 cultures as well as in Th2 cells post calcitriol stimulation.

411 Vitamin D deficiency differentially regulated the expression levels of several Chr17q12-21.1
412 encoded genes, with lower expression of *Ikzf3*, *Ormdl3* and *Gsdma* (all p=0.0286) (**Figure 2*D***).
413 Conversely, stimulation with calcitriol induced the expression of the same genes (all p=0.043)
414 (**Figure 2*E***). Expression of the Chr17q21.2 genes *Stat3*, *Stat5a* and *Stat5b* was not affected by
415 vitamin D deficiency (**Figure 2*F***). However, after calcitriol stimulation *Stat5a* (p=0.0082) and
416 *Stat5b* (p=0.003) genes were strongly suppressed and *Stat3* (p= 0.0048) expression was increased
417 in Th2 cells. (**Figure 2*G***). These results hint to a protective role of vitamin D in allergic airway
418 inflammation, by regulating the expression of the IL-2 downstream signaling molecules *Stat5a*
419 and *Stat5b*.

420

421 **Deficiency in vitamin D signaling augments allergic airway inflammation**

422 To decipher the protective role of vitamin D signaling in allergic airway inflammation, we
423 employed vitamin D deficient and $VDR^{-/-}$ mice (**Figure 3*A***) (28). HDM sensitization of vitamin

424 D deficient mice led to a stronger reaction to the allergen resulting in more prominent peri-
425 bronchial and perivascular leukocytic infiltrates (**Figure 3*B***). This phenotype was accompanied
426 by lower VDR expression in CD4+ T cells isolated from HDM-exposed lungs compared to WT
427 (**Figure 3*C***). Vitamin D deficiency led to a robust increase in total immunoglobulin (Ig)E levels
428 (**Figure 3*D***). Histological findings were associated with higher total BAL leukocyte (p= 0.0008)
429 (**Figure 3*E***), eosinophil (p= 0.0002) (**Figure 3*F***) and lymphocyte (p= 0.0023) (**Figure 3*G***)
430 numbers in vitamin D deficient mice. Th2 cell numbers (p= 0.0127) were also higher in the HDM
431 exposed mice (**Figure 3*H***) in a manner that was independent of T helper cell skewing (**Figure 3-**
432 **figure supplement 1*A, B***). Differentiation and recruitment of Th17 and IL-10 producing CD4+ T
433 cells was not affected by vitamin D deficiency (**Figure 3-figure supplement 1*A, B***). To validate
434 these findings from vitamin D deficiency, we next employed $VDR^{-/-}$ mice (see Methods). As with
435 the vitamin D deficient mice, HDM sensitization and challenge of $VDR^{-/-}$ mice led to an increased
436 Th2 immune response. The lung phenotype in the $VDR^{-/-}$ mice was marked by dense leukocytic
437 infiltrates around and mucus plugs in the airways (**Figure 3*B***). The augmented systemic and local
438 immune response increased total IgE titers (p= 0.0489), and total BAL (p< 0.0001 vs WT HDM
439 and p= 0.003 vs Vit D deficient HDM), eosinophil (p< 0.0001 vs WT HDM and Vit D deficient
440 HDM), total lymphocytes (p=0.0194 vs WT HDM and p= 0.0421vs Vit D deficient HDM) and
441 Th2 cells (p= 0.0009 vs WT HDM) (**Figure 3*D-H***). $VDR^{-/-}$ did not significantly affect recruitment
442 of Treg and Th17 cells (**Figure 3-figure supplement 1*A, B***).

443 To explore the mechanisms underlying the augmented Th2-phenotype in the lungs of vitamin D
444 deficient and $VDR^{-/-}$ mice after HDM allergen challenge, we analyzed the transcriptional profiles
445 of in vitro polarized Th2 cells from WT and vitamin D deficient mice (**Figure 3*I***). Differential
446 expression and enrichment analysis revealed dysregulation of several pathways implicated in Th2-

447 cell activation, cytokine production, proliferation, and survival with prominent changes in the IL-
448 2/ STAT5 - pathway in vitamin D deficient Th2 cells (p= 0.0014) (**Figure 3*J***, **Figure 3-table**
449 **supplements 1, 2**). The effects of impaired vitamin D signaling on these pathways was confirmed
450 by qRT-PCR and flow cytometry. Baseline expression of IL-2 was markedly increased at both the
451 RNA (p= 0.0286)) and protein levels (p= 0.0079) in vitamin D deficient and $VDR^{-/-}$ Th2 cells
452 (**Figure 3*K, L***). In Vitamin D deficient and $VDR^{-/-}$ Th2 cell *in vitro* incubation, the elevated IL-2
453 levels were accompanied by a sharp increase in IL-13 production (VitD deficient: p< 0.0001; VDR^{-}
454 $^{/-}$: p= 0.0141) (**Figure 3-figure supplement 2**).

455 Taken together, these results indicate a critical role for vitamin D/VDR signaling in regulating type
456 2 inflammation and identify the IL-2/ Stat5 pathway as a downstream target of vitamin D in Th2
457 cells.

458

459 **Vitamin D suppresses the activation of the IL-2/Stat5 pathway and cytokine production in**
460 **Th2 cells**

461 To ascertain the vitamin D dependent regulation of the IL-2/Stat5 pathway and the impact on the
462 effector program of Th2 cells, we first analyzed the transcriptional profile of WT Th2 cells exposed
463 to calcitriol during differentiation (**Figure 4*A***). Gene ontology enrichment analysis of biological
464 processes revealed regulation of several processes impacting inflammatory responses, including
465 chemotaxis and activation of cells (**Figure 4-table supplement 1**). Calcitriol stimulation of Th2
466 cells affected several immune related disease pathways, including asthma (**Figure 4-figure**
467 **supplement 1, Figure 4-table supplement 2**). Gene set enrichment analysis (GSEA), performed
468 on the differentially expressed genes, highlighted the negative regulation of IL-2/Stat5 pathway in
469 Th2 cells by calcitriol (**Figure 4*B***, **Figure 4-table supplement 3**). Calcitriol stimulation

470 suppressed the expression of *Il2* (p<0.0001), *Stat5a* (p<0.0008) and *Stat5b* (p<0.0008) genes
471 (**Figure 4*C***). Concordantly, levels of activated Itk (phospho-Itk) (p= 0.029) and expression of the
472 IL2Rβ (CD25) (p= 0.0441) were reduced on a per cell basis (**Figure 4*D***).

473

474 Next, the impact of calcitriol stimulation on the effector function of Th2 cells was assessed by
475 flow cytometric analysis for the T2 cytokine IL-13. Activation of the vitamin D/VDR pathway led
476 to significant suppression of IL-13 production in CD4+ T cells (p= 0.0012) (**Figure 4*E***).

477 To further delineate the molecular impact of vitamin D on Th2 cell biology, we integrated the
478 murine transcriptional profile with a recently developed human Protein-Protein Interaction (PPI)
479 database (34) . By modeling the signal transduction process as a sequential path on the PPI network
480 that starts from a receptor and propagates downstream to a transcription factor via multiple
481 intermediate proteins (for details see Methods section, **Figure 4-figure supplement 2*A***), we
482 inferred the active signaling flow in Th2 cells for control (vehicle) and calcitriol stimulated Th2
483 cells. As input of our network analysis, we selected a subset of receptors and transcription factors
484 that are known to be involved in CD4+ T cell activation, Th2 cell differentiation, and cytokine
485 production (**Figure 4-table supplement 4**). For clarity of the figure, we display the gene names.
486 Corresponding protein names are attached in **Figure 4-table supplement 5**. In control Th2 cells,
487 our network analysis revealed the engagement of a variety of receptors including IL4R, IL2RA,
488 CD28, and TNF-receptors. Downstream to these receptors, the most active signaling paths
489 highlighted the activation of STAT3, STAT5A/B, NFkB1, and IKZF1 transcription factors
490 (**Figure 4-figure supplement 2*B***) via multiple adapter proteins of the TRAF and JAK family.
491 Interestingly, these transcription factors are known to be involved in differentiation and activation
492 pathways in Th2 cells Conversely, after calcitriol stimulation, signal from IL4R, CD28 and

493 TNFSF8 propagated over different interaction partners (**Figure 4*F***). Calcitriol specific edges are
494 highlighted in orange color. Molecular mediators included the cytoskeletal proteins VAV1 and
495 RACK1 and emphasized activation of the transcription factors AP-1 (FOS/JUND dimer) and
496 NFATC1.
497
498 Our network analysis highlighted a central role of the transcriptional repressor IKZF1 (IKAROS)
499 upon calcitriol stimulation, which was targeted by multiple downstream mediators including
500 IKZF3 (AIOLOS). Notably, the IKZF3 gene encodes for the AIOLOS protein, a direct interaction
501 partner of the IKZF1-encoded IKAROS. Both transcription factors, as homo- and heterodimers,
502 suppress IL-2 expression on the transcriptional levels in mouse and human lymphocytes (44).
503 Calcitriol increased the number of edges connecting intermediate proteins to the transcriptional
504 repressor IKAROS. Among the connecting proteins, AIOLOS interaction with IKAROS was
505 implicated in repression of IL-2 expression in Th2 cells by vitamin D.
506 Absence of STAT5A/B mediators in the active signaling paths of calcitriol stimulated Th2 cells
507 further suggested repression of the Th2 cell STAT5 pathway with calcitriol compared to control
508 (**Figure 4-figure supplement 2*B***).
509
510 Taken together, these results indicate that the specific suppression of the IL-2/Stat5 pathway by
511 vitamin D results in reduced cytokine production by Th2 cells. Our findings suggest that this
512 suppression was mediated by the vitamin D dependent regulation of IKAROS (IKZF1) through
513 the induction of AIOLOS (IKZF3).
514

515 **Vitamin D supplementation alleviates the allergic phenotype in the lung by suppressing type**
516 **2 cytokine production in a dose dependent manner**

517 To test if vitamin D supplementation prevents the development of T2 driven allergic inflammation
518 in the lung, custom rodent diets with select vitamin D doses were used: 400 IU/kg chow (400 IU;
519 low), 1000 IU/kg chow (1000 IU; regular) and 4000 IU/kg chow (4000 IU; high) (**Figure 5- figure**
520 **supplement 1*A*,** see Methods section). The 1000 IU group was used as the control group, as it
521 contains the average amount of vitamin D fortified in standard rodent chow. HDM exposure led
522 to recruitment of leukocytes into the lung tissue and BAL (**Figure 5*A, B***), with a predominant
523 eosinophilic and lymphocytic infiltrate as well as high numbers of IL-13+ Th2 cells (**Figure 5*C-***
524 ***E***). There were trends for higher cellular infiltration in the airways when mice were supplemented
525 with the low vitamin D doses (400 IU), but these inflammatory responses were not significantly
526 different from the phenotype observed with 1000 IU. Lung and airway pathology were similar
527 between these dosing groups, with similar numbers and frequencies of the different leukocyte
528 populations. In sharp contrast, dietary supplementation with the higher vitamin D dose (4000 IU)
529 decreased the inflammatory phenotype in HDM exposed mice compared to the 400 IU and 1000
530 IU dosed animals. Concordant with the histological findings, BAL leukocytes ($p< 0.0001$) were
531 decreased with marked reductions in BAL eosinophil ($p=0.0016$) and lymphocyte numbers
532 ($p=0.026$) (**Figure 5*B, D***), and the frequency of IL-13+ Th2 cells was significantly reduced in the
533 lungs with 4000 IU of vitamin D ($p= 0.0066$ vs 400 IU HDM; $p=0.0011$ vs 1000 IU HDM) (**Figure**
534 **5*E***). Of note, dietary supplementation with high vitamin D levels, increased VDR expression in
535 CD4+ T cells from HDM exposed lungs ($p< 0.0001$) (**Figure 5- figure supplement 1*B***).

536 To ascertain that dietary supplementation with vitamin D specifically altered mouse Th2 cell
537 differentiation and the effector program, splenic naïve CD4+ T cells from 400 IU and 4000 IU

538 mice were studied. Of interest, naïve CD4+ T cells did not express VDR until they were exposed
539 to Th2 polarizing conditions. Gata3 expression on per cell basis was lower in 4000 IU Th2 cells
540 (p= 0.0286) (**Figure 5- figure supplement 2*A***). This was accompanied by higher VDR protein
541 expression (p= 0.0286) (**Figure 5- figure supplement 2*B***). The expression of IL-2 (p= 0.0004)
542 and the Th2 cytokines IL-13 (p= 0.0159) and IL-5 (p= 0.0159) were lower in 4000 IU Th2 cultures
543 (**Figure 5- figure supplement 2*C-E***).

544 To explore the specific induction of Aiolos expression for vitamin D mediated suppression of IL-
545 2 production in Th2 cells, Aiolos expression was monitored throughout Th2 differentiation. Aiolos
546 expression gradually increased under Th2 polarizing conditions in CD4+ T cells, starting as early
547 as day 1 of in vitro culture (**Figure 5*F***). Simultaneous exposure to calcitriol further increased
548 Aiolos protein levels compared to vehicle in Th2 cells (p= 0.0079) (**Figure 5*G***).

549 To test if vitamin D exerts its inhibitory effect on IL-2 production via Aiolos induction, Ikzf3$^{-/-}$
550 mice were employed, exposed to Th2 polarizing conditions and assessed for IL-2 production after
551 calcitriol exposure. IL-2 production in control Ikzf3$^{-/-}$ Th2 cultures was significantly higher
552 compared to WT Th2 cells. Calcitriol significantly reduced IL-2 levels in both, WT (p= 0.0001)
553 and Ikzf3$^{-/-}$ Th2 cells (p= 0.0001) (**Figure 5*H***); however, the suppressive effect of calcitriol on IL-
554 2 production was significantly higher in WT Th2 cells (~ 65% inhibition) compared to Ikzf3$^{-/-}$ Th2
555 cells (~40% inhibition) (p= 0.0001) (**Figure 5*H***).

556 Taken together, these results indicated that vitamin D can regulate Aiolos expression and
557 suggested a role for Aiolos as a downstream effector for selectively fine-tuning Th2 cell IL-2
558 production by vitamin D.

559

560 **DISCUSSION**

561 We utilized human genetics to identify SNPs on chromosome 17q12-21.1 and 17q21.2 that were
562 within GWAS regions for Th1 and Th2 autoimmune diseases. Of note, many of these SNPs were
563 within VDR binding sites. We then determined by eQTL analysis of the genes in these two
564 genomic regions that IKZF3 expression was controlled by four cis-eQTLs in the enhancer region
565 targeting ORMDL3 and IKZF3, and in the enhancer region targeting ORMDL3, GSDMA and
566 GSDMB. Next, we demonstrated that two SNPs in CTCF binding sites were in strong LD with
567 these 4 eQTL SNPs and that the two enhancer sites in 17q12-21.1 were both predicted to interact
568 with the ORMDL3 promoter region, and the enhancer site in 17q21.2 was predicted to interact
569 with the STAT5A promoter region thus, suggesting a plausible human molecular genetic
570 mechanism by which vitamin D could activate IKZF3 to repress ORMDL3 and immune system
571 development. Finally, we leveraged bulk RNAseq in the cord blood of the VDAART trial to show
572 that an interaction for vitamin D level and IKZF3 expression that was associated with reduced
573 asthma risk at 3 years of age.

574 To confirm our human molecular genetic findings, we chose to utilize mouse models of allergic
575 lung inflammation. We show strong VDR expression in CD4+ Th2 cells and alterations in
576 chr17q12-21.1 and 17q21.2 gene expression induced by vitamin D status. Expression of VDR has
577 been reported for airway epithelial cells and different immune cell types present in the lung (45).
578 In lymphocytes, *ex vivo* and *in vitro* studies describe low baseline VDR transcript expression levels
579 that were transiently increased by activating signals and calcitriol stimulation (46). Here, we report
580 a differential VDR expression pattern in CD4+ T cell subsets in allergic inflamed lungs and post
581 lineage specific cytokine stimulation *in vitro*, with strongest expression in Th2 cells. Activation of
582 VDR suppressed IL-2, IL-5, and IL-13 production by Th2 cells. The expression of VDR in
583 Gata3+Th2 cells in the lung might represent an endogenous control mechanism to curb the

584 pathogenic cell activity and cytokine production after repetitive allergen contact. *Ex vivo* and *in*
585 *vitro* Th1, nTreg and iTreg cells expressed low VDR protein levels at baseline. It remains to be
586 determined whether other Th-subsets described in allergic inflammation express VDR at baseline
587 and if either calcitriol or other secondary signals, specific for each subset, could induce VDR
588 expression during inflammation.

589 Vitamin D deficiency that had been introduced over two generations and impaired vitamin D
590 signaling led to an augmented allergic phenotype in the lung after allergen exposure with a
591 dominating Th2-signature locally and systemically. This had likely been due to specific
592 deregulation of Th2 cells instead of Th cell skewing, since neither Th17 nor Treg development
593 and recruitment had been significantly affected. In contrast, in mice supplemented with high
594 vitamin D doses over two generations, VDR expression and consequently vitamin D
595 responsiveness was higher in CD4+ T cells from the animals' lungs, almost abrogating the
596 inflammatory process in the lung after allergen challenge. While the vitamin D dose had been
597 chosen to replicate the VDAART trial in the mouse, the duration of supplementation was adopted
598 to the protocol of generating vitamin D deficient mice. Both factors might influence the outcome
599 here compared to prior rodent studies with inconclusive results.

600 Differentiation of Th2 cells is driven by IL-4 induced Gata3 expression in naïve CD4+ T cells.
601 This process depends on a positive feedforward loop by IL-2 and its downstream STAT5 signaling
602 pathway for the effective expression of IL-4 (47). Therefore, either interfering with Gata3
603 expression or the IL-2 pathway represents a promising strategy to finetune Th2-driven immunity.
604 Our data highlight the specific regulation of the IL-2/STAT5 pathway by vitamin D. Vitamin D
605 deficiency and impaired VDR signaling caused elevated IL-2 production by Th2 cells, mounting
606 in high IL-13 production. Elevated IL-13 levels *in vivo*, could amplify the local T2 responses in

607 the lung. In sharp contrast, exposure of polarizing Th2 cells to calcitriol was able to suppress IL-2
608 production, expression and activation of STAT5A/B and therefore IL-13 production by Th2 cells.
609 The transcription factor AIOLOS has previously been shown to suppress IL-2 expression on the
610 transcriptional level(44). We report here a vitamin D mediated induction of Aiolos expression in
611 Th2 cells, which is impaired by vitamin D deficiency. High Aiolos expression coincided with
612 lower IL-2 production, ameliorated STAT5A/B expression, and IL-13 production in Th2 cells. *In*
613 *vitro* Th2 polarization of naïve CD4+ T cells isolated from mice supplemented with higher vitamin
614 D levels, without further exogenous calcitriol stimulation, developed a weakened Th2 phenotype,
615 characterized by lower IL-2, IL-5, and IL-13 production. Since naïve CD4+ T cells do not express
616 VDR, these results implicate changes in chromosomal accessibility by high vitamin D in the
617 developing immune system, which needs further investigation.

618 Experiments here with Ikzf3$^{-/-}$ mice demonstrated significant reductions in vitamin D mediated
619 control of Th2 cell cytokine production, but the vitamin D response was not completely impaired,
620 suggesting additional mechanisms for vitamin D regulation of Th2 cells – several possibilities
621 were uncovered by our PPI analyses. These will be the subject of future research. In addition, we
622 only investigated a Th2 mouse model of asthma and have not extended our mouse work to Th1
623 models of autoimmunity. We have still to consider other genes that might be linked to these two
624 genetic loci and there are likely other VDR binding sites of importance in both asthma and Th1
625 autoimmunity. More work to determine the exact levels of vitamin D that confer this protective
626 effect would also be worthy of further investigation.

627 In summary, we have leveraged clinical trial data, molecular genetic bioinformatic data and mouse
628 model data to outline for the first time, a comprehensive molecular genetic mechanism for how
629 vitamin D influences not only asthma, but both Th1 and Th2 autoimmune disease. The significance

630 of these findings relates to the high prevalence of vitamin D deficiency, especially during
631 pregnancy, and the strong possibility that the epidemic of asthma and autoimmunity might be
632 significantly reduced if vitamin D levels were elevated worldwide.

633

634 **List of Supplementary Materials**

635 Fig S1 to S11

636 Tables S1 to S9

637

638 **Acknowledgments:** We wish to thank the VDAART trial participants and clinical staff for their
639 critical work on the VDAART study. We wish to thank also our Channing colleagues for
640 their comments.

641 **Funding:**

642 National Heart, Lung, and Blood Institute grant 5P01HL132825
643 National Heart, Lung, and Blood Institute grant 5UH3OD023268
644 National Heart, Lung, and Blood Institute grant 5K25HL150336
645 German Society for Clinical Chemistry and Laboratory Medicine (DGKL) and the
646 German Research Foundation (DFG) grant KI 1868/3-1

647 **Author contributions:**

648 A.K. and S.T.W. jointly supervised this work. A.K. and S.T.W. designed the experiments,
649 analyzed data, and wrote the manuscript. A.K., M.G.D., T.R.B., J.R.Q., A.O.S, J.K., T.N., H.Y.P.,
650 N.K. and R.E.A performed experiments. A.H., E.M., M.D.M. and R. C. analyzed data. M.D. and
651 K.G. provided critical mouse lines and scientific input. A.A.L. assisted on VDAART related

652 analyses. H.R. and B.D.L. supervised experiments and provided critical scientific input. All
653 authors critically reviewed the manuscript.

654 **Competing interests:** Dr. Weiss receives royalties from UpToDate and is an investor in Histolix.
655 All other authors declare that they have no competing interests.

656 **Data and materials availability:** All data are available in the main text or the supplementary
657 materials.

658

659 **Figure legends**

660 **Figure 1. VDR binding sites on Chr17q12 and q21.1 overlap with open chromatin signatures.**
661 ***A***, Significant disease and trait associations in 17q12-21.1 (y-axis), retrieved from the NHGRI EBI
662 GWAS Catalog, with at least one significant SNP (x-axis) in Chr17q12-21.1. Colored bars denote
663 autoimmune diseases mapped to Th1 (red bars) or Th2 (blue bars) driven immunity. ***B***, University
664 of California Santa Cruz (UCSC) Genome Browser tracks showing chromosomal location,
665 common dbSNPs, VDR-, RXR-, CTCF- and IKZF3-binding sites and H3K27Ac marks present in
666 the Chr17q12-21.1 locus. VDR binding sites overlapping with active regulatory elements are
667 highlighted by colored boxes. ***C***, Linkage disequilibrium (LD) between the significant SNPs in the
668 Chr17q12-21.1 (magenta) and 21.2 (green) region, highlighting Th1/Th2 associated SNPs (red and
669 blue, respectively), eQTLs in the VDR binding regions in Chr17q12 21.1 and 21.2 (yellow), and
670 functional asthma SNPs from the literature (cyan).

671

672 **Figure 1-figure supplement 1. *A*,** Significant disease and trait associations in 17q21.2 (y-axis),
673 retrieved from the NHGRI-EBI GWAS Catalog, with at least one significant SNPs (x-axis) in

674 Chr17q21.2. Colored bars denote autoimmune diseases mapped to Th1 (red bars) or Th2 (blue
675 bars) driven immunity. ***B*,** University of California Santa Cruz (UCSC) Genome Browser tracks
676 showing chromosomal location, common dbSNPs, VDR-, RXR-, CTCF- and IKZF3-binding sites
677 and H3K27Ac marks present in the Ch17q21.2 locus. VDR binding sites overlapping with active
678 regulatory elements are highlighted by colored boxes.

679

680 **Figure 2. VDR expression is elevated in Th2 cells and vitamin D regulated expression of genes**
681 **on Chr1q12 and Chr17q21.** *A*, Scheme of the house dust mite (HDM) induced airway
682 inflammation protocol. ***A*,** Flow cytometric analysis and cell frequencies of VDR expression in
683 CD45+ CD4+ T cells in the respective groups (n=4-5). ***C*,** Flow cytometric analyses and cell
684 frequencies of VDR expression in Th1 (Tbet+), Th2 (Gata3+) and Treg (Foxp3+) cells in the
685 respective groups (n=4-7). Quantitative RT-PCR analysis of relative mRNA expression levels of
686 genes encoded on Chr17q12-21.1 in (***D***) Th2 cultures of WT and vitamin D deficient mice and (***E***)
687 control and calcitriol stimulated cultures. Quantitative RT-PCR analysis of relative mRNA
688 expression levels of genes encoded on Chr17q21.2 in (***F***) Th2 cultures of WT and vitamin D
689 deficient mice and (***G***) control and calcitriol stimulated cultures. Gene expression levels were
690 normalized to the house keeping gene L32 and are expressed relative to the expression level in
691 WT (***D, F***) or WT-vehicle (***E, G***) Th2 cells. ($n \geq 4$ per group). Each symbol represents one mouse.
692 Numbers in flow plots indicate percentages. Error bars indicate the s.e.m. Statistical tests: two-

693 tailed Mann-Whitney U test (***B, C***). *P < 0.05, **P < 0.01, ***P < 0.001. Data summarize results
694 from two independent experiments.

695

696 **Figure 2-figure supplement 1. Baseline VDR expression is confined to the CD4+ Foxp3- Teff**
697 **cell population.** ***A***, Gating strategy for the analysis of VDR expression in different leukocyte
698 populations in the lung. ***B*****,** Flow cytometric analysis and cell frequencies of VDR expression in
699 CD45+, CD4+, CD8+ and CD19+ in the respective groups (n=4-5). ***C*****,** Representative flow plots
700 of lung CD45+ CD4+ T cells isolated from saline and HDM- immunized and -challenged mice for
701 the co-expression of Foxp3 and VDR. Each symbol represents one mouse. Numbers in flow plots
702 indicate percentages. Error bars indicate the s.e.m. Statistical tests: two-tailed Mann-Whitney U
703 test. *P < 0.05. Data summarize results from two independent experiments.

704

705 **Figure 2-figure supplement 2. VDR expression is induced during CD4+ Th2 cell**
706 **differentiation**. ***A*****,** Representative immunoblot for VDR expression in freshly isolated (0 hrs) and
707 activated CD4+ CD62L+ CD44- naïve T cells (48 hrs.) and in vitro polarized Th1, Th2 and iTreg
708 cells. Kidney samples of WT and VDR-/- mice were used as controls. ***B*****,** Representative
709 immunoblot for VDR expression in polarizing Th2 at the indicated days of in vitro culture. ***C*****,**
710 Representative image of VDR localization in in vitro polarized Th2 cells stimulated with vehicle
711 (EtOH, [% v/v]) or calcitriol.

712

713 **Figure 3. Vitamin D deficiency augments allergic airway inflammation.** ***A,*** Schematic
714 presentation of the different mouse strains used. ***B,*** Representative H&E-stained lung sections

715 from saline and HDM-exposed wild type (C57/BL6; WT), vitamin D deficient and VDR-/- mice
716 (x 10 magnification). Black arrows point to the peri bronchial infiltrate. ***C,*** Representative flow
717 plots assessing VDR expression in lung CD4+ T cells from the indicated groups. ***D,*** Total IgE
718 levels detected in the sera of respective groups. ***E-G,*** Absolute numbers of (***E***) leukocytes, (***F***)
719 eosinophils, and (***G***) lymphocytes in the airways of the respective groups. ***H,*** Frequencies of IL-
720 13 producing Th2 in the lung. Data summarize results from two or three independent experiments
721 with n>8 per group. ***I,*** Heat map showing differentially expressed genes between WT and vitamin
722 D deficient Th2 cultures identified by RNA-Sequencing analysis. Analysis and visualization were
723 performed with DESeq2. ***J,*** Overrepresentation analysis of Hallmark gene sets in the differentially
724 expression gene set. The x-axis represents the gene ratio in the respective gene set. Dot sizes denote
725 the number of genes in the respective pathway. The dot color indicates the FDR-adjusted p-value.
726 Analysis and visualization were performed with the clusterProfiler package. ***K,*** Quantitative RT-
727 PCR analysis of Il-2 mRNA expression in Th2 cultures from the respective groups (n=4 per group).
728 Gene expression levels were normalized to the house keeping gene L32 and are expressed as fold-
729 induction compared to WT Th2 cells. ***L***, Flow cytometric analysis and cell frequencies of IL-2
730 production in WT and VDR-/- Th2 cultures (n=5 per group). Each symbol represents one mouse.
731 Error bars indicate the s.e.m. Statistical significance was determined with: Mixed-effect analysis
732 with Holm-Šidák's post-hoc analysis (***D –H***), two-tailed Mann-Whitney U test (***K, L***). *P < 0.05,
733 **P < 0.01, ***P < 0.001, ****P < 0.0001. Data summarize results from two or three independent
734 experiments with n>8 per group.

735

736 **Figure 3-figure supplement 1. Vitamin D deficiency does not alter CD4+ IL-10 and IL-17A**
737 **expression allergic airway inflammation.** Frequencies of IL-10 (***A***) and IL-17A (***B***) CD4+ T

738 cells. Each symbol represents one mouse. Error bars indicate the s.e.m. Data summarize results
739 from two or three independent experiments with n>8 per group.

740

741 **Figure 3-figure supplement 2. Vitamin D deficiency increases IL-13 expression in Th2 cells.**
742 Flow cytometric analysis and frequencies of IL-13 expression in WT, vitamin D deficient and
743 VDR-/- Th2 cultures (n=5-9 per group). Each symbol represents one individual sample and data
744 summarize the results from two or three independent experiments. Error bars indicate the s.e.m.
745 Statistical tests: Kruskal- Wallis Test with Dunn's post-hoc analysis. *P < 0.05, **P < 0.01, ****P
746 < 0.0001.

747

748 **Figure 4. Vitamin D stimulation of polarizing Th2 cells suppresses the IL-2/Stat5 pathway.**
749 ***A***, Heat map of differentially expressed genes between vehicle (EtOH [% v/v]) and calcitriol
750 treated WT Th2 cells. Analysis and visualization were performed with DESeq2. ***B***, Gene set
751 enrichment analysis (GSEA) of differentially expressed genes. Analysis and visualization were
752 performed with the clusterProfiler package. ***C***, Quantitative RT-PCR for Il-2, Stat5a and Stat5b
753 mRNA expression in Th2 cells exposed to either vehicle or calcitriol. Gene expression levels were
754 normalized to the house keeping gene L32 and are expressed as fold-induction compared to control
755 cells. ***D***, Flow cytometric analysis and mean fluorescence intensities of Itk and Il2rβ expression in
756 indicated groups. ***E***, Flow cytometric analysis and quantification of IL-13 expression in respective
757 groups. ***F***, Network analysis to visualize vitamin D induced molecular changes in the molecular
758 interactome of calcitriol stimulated CD4+ Th2. Predefined set of cell membrane receptors were
759 set as starting points (orange nodes) and annotated transcription factors were set as ending points
760 (blue). All intermediate proteins on the PPI are visualized as grey nodes. Molecular interactions

761 only overrepresented in calcitriol stimulated cells are shown as orange arrows. Each symbol in the
762 bar graphs represents one individual sample and data summarize the results from two or three
763 independent experiments with n≥ 5. Error bars indicate the s.e.m. Statistical test: two-tailed
764 Student's t-test (***C, E***) and two-tailed Mann-Whitney U-test (D). *P < 0.05, **P < 0.01, ***P <
765 0.001.

766

767 **Figure 4-figure supplement 1. KEGG pathways analysis post vitamin D stimulation.** List of
768 KEGG pathways enriched (p-adj. < 0.05) in DE genes after calcitriol stimulation. The x-axis
769 indicates the number of genes annotated to each pathway. The bar colors indicate the FDR-adjusted
770 p-value based on the colormap on the right side of the figure. The R package clusterProfiler was
771 used for the enrichment analysis and visualization.

772

773 **Figure 4-figure supplement 2. Active signaling pathways in Th2 cells.** ***A***, Schematic
774 representation of the network analysis employed. ***B***, Network analysis to visualize active signaling
775 paths in control stimulated Th2 cultures. Predefined set of cell membrane receptors were set as
776 starting points (orange nodes) and annotated transcription factors were set as ending points (blue).
777 All intermediate proteins on the PPI are visualized as grey nodes. Molecular interactions only
778 overrepresented in control stimulated cells are shown as purple arrows.

779

780 **Figure 5. Prenatal vitamin D supplementation protects from asthma development.** ***A*,** H&E
781 staining of representative lung sections of indicated experimental groups. Arrowheads point to peri
782 bronchial infiltrates. ***B-E*,** Absolute numbers of total BAL (***B***) leukocytes, (***C***) eosinophils, (***D***)

783 lymphocytes, and (***E***) lung IL-13+ Th2 cells. ***F,*** Flow cytometric analysis of Aiolos expression in
784 differentiating Th2 cells at indicated time points. ***G***, QRT-PCR analysis of Ikzf3 transcripts in
785 respective groups. Expression levels were normalized to the house keeping gene L32 and are
786 expressed as fold change expression over the control samples WT-vehicle/ WT. ***H***, Flow
787 cytometric analysis of Aiolos expression in control and calcitriol stimulated Th2 cells. ***I,*** Flow
788 cytometric analysis and frequencies of IL-2+ cells in WT and Ikzf3-/- cultures post indicated
789 treatment. Each symbol represents and independent sample (n= 9 per group). Flow cytometric
790 analysis and quantification of VDR expression in lung CD4+ T cells of the respective groups. Each
791 symbol represents one individual mouse and data summarize the results from two to three
792 independent experiments with n>8 per group. Error bars indicate the s.e.m. Statistical significance
793 was determined with Mixed-effect analysis with Holm-Šidák's post-hoc analysis (***B-E***), two-tailed
794 Mann-Whitney U-test (***G, H***) and One-way ANOVA with Holm-Šidák's post-hoc analysis (***G***). *P
795 < 0.05, **P < 0.01, ***P < 0.001, ****P < 0.0001.

796

797 **Figure 5-figure supplement 1. Prenatal vitamin D supplementation increases VDR**
798 **expression in CD4+ T cells.** ***A***, Schematic presentation of the dietary intervention protocol and
799 breeding scheme with vitamin D. ***B***, Flow cytometric analysis and quantification of VDR
800 expression in lung CD4+ T cells of the respective groups. Each symbol represents one individual
801 mouse and data summarize the results from two to three independent experiments with n>8 per
802 group. Error bars indicate the s.e.m. Statistical significance was determined with One-way
803 ANOVA with Holm-Šidák's post-hoc analysis. *P < 0.05, **P < 0.01, ***P < 0.001, ****P <
804 0.0001.

805

806 **Figure 5-figure supplement 2. Prenatal vitamin D supplementation mitigates Th2**
807 **development and cytokine production in vitro.** ***A-E***, Representative flow plots and cell
808 frequencies of (***A***) Gata3, (***B***) VDR, (***C***), IL-2, (***D***) IL-13, (***E***) IL-5 expression in indicated groups.
809 Each symbol represents one individual sample and data summarize the results from two to three
810 independent experiments (n= 4-5 per group). Error bars indicate the s.e.m. Statistical test: two-
811 tailed Mann-Whitney U-test (**a – e**). *P < 0.05, **P < 0.01, ***P < 0.001.

812

813 Literature Cited

814 1. Litonjua AA, Weiss ST. Is vitamin D deficiency to blame for the asthma epidemic? J Allergy
815 Clin Immunol 2007; 120(5):1031–5.
816 2. Bouzigon E, Corda E, Aschard H, Dizier M-H, Boland A, Bousquet J et al. Effect of 17q21
817 variants and smoking exposure in early-onset asthma. N Engl J Med 2008; 359(19):1985–94.
818 3. Kelly RS, Chawes BL, Guo F, Zhang L, Blighe K, Litonjua AA et al. The role of the 17q21
819 genotype in the prevention of early childhood asthma and recurrent wheeze by vitamin D. Eur
820 Respir J 2019; 54(4).
821 4. Schmiedel BJ, Seumois G, Samaniego-Castruita D, Cayford J, Schulten V, Chavez L et al.
822 17q21 asthma-risk variants switch CTCF binding and regulate IL-2 production by T cells. Nat
823 Commun 2016; 7:13426.

824 5. Raby BA, Lazarus R, Silverman EK, Lake S, Lange C, Wjst M et al. Association of vitamin D
825 receptor gene polymorphisms with childhood and adult asthma. Am J Respir Crit Care Med
826 2004; 170(10):1057–65.
827 6. Camargo CA, Rifas-Shiman SL, Litonjua AA, Rich-Edwards JW, Weiss ST, Gold DR et al.
828 Maternal intake of vitamin D during pregnancy and risk of recurrent wheeze in children at 3 y of
829 age. Am J Clin Nutr 2007; 85(3):788–95.
830 7. Devereux G, Litonjua AA, Turner SW, Craig LCA, McNeill G, Martindale S et al. Maternal
831 vitamin D intake during pregnancy and early childhood wheezing. Am J Clin Nutr 2007;
832 85(3):853–9.
833 8. van der Pligt P, Willcox J, Szymlek-Gay EA, Murray E, Worsley A, Daly RM. Associations
834 of Maternal Vitamin D Deficiency with Pregnancy and Neonatal Complications in Developing
835 Countries: A Systematic Review. Nutrients 2018; 10(5).
836 9. Roth DE, Abrams SA, Aloia J, Bergeron G, Bourassa MW, Brown KH et al. Global
837 prevalence and disease burden of vitamin D deficiency: a roadmap for action in low- and middle-
838 income countries. Ann N Y Acad Sci 2018; 1430(1):44–79.
839 10. Cashman KD. Vitamin D Deficiency: Defining, Prevalence, Causes, and Strategies of
840 Addressing. Calcif Tissue Int 2020; 106(1):14–29.
841 11. Litonjua AA, Lange NE, Carey VJ, Brown S, Laranjo N, Harshfield BJ et al. The Vitamin D
842 Antenatal Asthma Reduction Trial (VDAART): rationale, design, and methods of a randomized,
843 controlled trial of vitamin D supplementation in pregnancy for the primary prevention of asthma
844 and allergies in children. Contemp Clin Trials 2014; 38(1):37–50.

845 12. Litonjua AA, Carey VJ, Laranjo N, Harshfield BJ, McElrath TF, O'Connor GT et al. Effect
846 of Prenatal Supplementation With Vitamin D on Asthma or Recurrent Wheezing in Offspring by
847 Age 3 Years: The VDAART Randomized Clinical Trial. JAMA 2016; 315(4):362–70.
848 13. Litonjua AA, Carey VJ, Laranjo N, Stubbs BJ, Mirzakhani H, O'Connor GT et al. Six-Year
849 Follow-up of a Trial of Antenatal Vitamin D for Asthma Reduction. N Engl J Med 2020;
850 382(6):525–33.
851 14. Wolsk HM, Chawes BL, Litonjua AA, Hollis BW, Waage J, Stokholm J et al. Prenatal
852 vitamin D supplementation reduces risk of asthma/recurrent wheeze in early childhood: A
853 combined analysis of two randomized controlled trials. PLoS One 2017; 12(10):e0186657.
854 15. Wolsk HM, Harshfield BJ, Laranjo N, Carey VJ, O'Connor G, Sandel M et al. Vitamin D
855 supplementation in pregnancy, prenatal 25(OH)D levels, race, and subsequent asthma or
856 recurrent wheeze in offspring: Secondary analyses from the Vitamin D Antenatal Asthma
857 Reduction Trial. J Allergy Clin Immunol 2017; 140(5):1423-1429.e5.
858 16. Verlaan DJ, Berlivet S, Hunninghake GM, Madore A-M, Larivière M, Moussette S et al.
859 Allele-specific chromatin remodeling in the ZPBP2/GSDMB/ORMDL3 locus associated with
860 the risk of asthma and autoimmune disease. Am J Hum Genet 2009; 85(3):377–93.
861 17. Miller M, Rosenthal P, Beppu A, Mueller JL, Hoffman HM, Tam AB et al. ORMDL3
862 transgenic mice have increased airway remodeling and airway responsiveness characteristic of
863 asthma. J Immunol 2014; 192(8):3475–87.
864 18. Zhang Y, Willis-Owen SAG, Spiegel S, Lloyd CM, Moffatt MF, Cookson WOCM. The
865 ORMDL3 Asthma Gene Regulates ICAM1 and Has Multiple Effects on Cellular Inflammation.
866 Am J Respir Crit Care Med 2019; 199(4):478–88.

867 19. Fishilevich S, Nudel R, Rappaport N, Hadar R, Plaschkes I, Iny Stein T et al. GeneHancer:
868 genome-wide integration of enhancers and target genes in GeneCards. Database (Oxford) 2017;
869 2017.
870 20. Neme A, Seuter S, Carlberg C. Vitamin D-dependent chromatin association of CTCF in
871 human monocytes. Biochim Biophys Acta 2016; 1859(11):1380–8.
872 21. Neme A, Seuter S, Carlberg C. Selective regulation of biological processes by vitamin D
873 based on the spatio-temporal cistrome of its receptor. Biochim Biophys Acta Gene Regul Mech
874 2017; 1860(9):952–61.
875 22. Ramagopalan SV, Heger A, Berlanga AJ, Maugeri NJ, Lincoln MR, Burrell A et al. A ChIP-
876 seq defined genome-wide map of vitamin D receptor binding: associations with disease and
877 evolution. Genome Res 2010; 20(10):1352–60.
878 23. Lu X, Chu C-S, Fang T, Rayon-Estrada V, Fang F, Patke A et al. MTA2/NuRD Regulates B
879 Cell Development and Cooperates with OCA-B in Controlling the Pre-B to Immature B Cell
880 Transition. Cell Rep 2019; 28(2):472-485.e5.
881 24. Buniello A, MacArthur JAL, Cerezo M, Harris LW, Hayhurst J, Malangone C et al. The
882 NHGRI-EBI GWAS Catalog of published genome-wide association studies, targeted arrays and
883 summary statistics 2019. Nucleic Acids Res 2019; 47(D1):D1005-D1012.
884 25. Dobin A, Davis CA, Schlesinger F, Drenkow J, Zaleski C, Jha S et al. STAR: ultrafast
885 universal RNA-seq aligner. Bioinformatics 2013; 29(1):15–21.
886 26. Anders S, Pyl PT, Huber W. HTSeq--a Python framework to work with high-throughput
887 sequencing data. Bioinformatics 2015; 31(2):166–9.
888 27. McCarthy DJ, Chen Y, Smyth GK. Differential expression analysis of multifactor RNA-Seq
889 experiments with respect to biological variation. Nucleic Acids Res 2012; 40(10):4288–97.

890 28. Sakai Y, Kishimoto J, Demay MB. Metabolic and cellular analysis of alopecia in vitamin D
891 receptor knockout mice. J Clin Invest 2001; 107(8):961–6.
892 29. Li YC, Amling M, Pirro AE, Priemel M, Meuse J, Baron R et al. Normalization of mineral
893 ion homeostasis by dietary means prevents hyperparathyroidism, rickets, and osteomalacia, but
894 not alopecia in vitamin D receptor-ablated mice. Endocrinology 1998; 139(10):4391–6.
895 30. Love MI, Huber W, Anders S. Moderated estimation of fold change and dispersion for RNA-
896 seq data with DESeq2. Genome Biol 2014; 15(12):550.
897 31. Yu G, Wang L-G, Han Y, He Q-Y. clusterProfiler: an R package for comparing biological
898 themes among gene clusters. OMICS 2012; 16(5):284–7.
899 32. Ritchie ME, Phipson B, Di Wu, Hu Y, Law CW, Shi W et al. limma powers differential
900 expression analyses for RNA-sequencing and microarray studies. Nucleic Acids Res 2015;
901 43(7):e47.
902 33. Benjamini Y, Drai D, Elmer G, Kafkafi N, Golani I. Controlling the false discovery rate in
903 behavior genetics research. Behav Brain Res 2001; 125(1-2):279–84.
904 34. Silverbush D, Sharan R. A systematic approach to orient the human protein-protein
905 interaction network. Nat Commun 2019; 10(1):3015.
906 35. Smedley D, Haider S, Durinck S, Pandini L, Provero P, Allen J et al. The BioMart
907 community portal: an innovative alternative to large, centralized data repositories. Nucleic Acids
908 Res 2015; 43(W1):W589-98.
909 36. Moffatt MF, Kabesch M, Liang L, Dixon AL, Strachan D, Heath S et al. Genetic variants
910 regulating ORMDL3 expression contribute to the risk of childhood asthma. Nature 2007;
911 448(7152):470–3.

912 37. Litherland SA, Xie TX, Grebe KM, Davoodi-Semiromi A, Elf J, Belkin NS et al. Signal
913 transduction activator of transcription 5 (STAT5) dysfunction in autoimmune monocytes and
914 macrophages. J Autoimmun 2005; 24(4):297–310.
915 38. Kara S, Pirela-Morillo GA, Gilliam CT, Wilson GD. Identification of novel susceptibility
916 genes associated with seven autoimmune disorders using whole genome molecular interaction
917 networks. J Autoimmun 2019; 97:48–58.
918 39. Syreeni A, Sandholm N, Sidore C, Cucca F, Haukka J, Harjutsalo V et al. Genome-wide
919 search for genes affecting the age at diagnosis of type 1 diabetes. J Intern Med 2021;
920 289(5):662–74.
921 40. Shrine N, Portelli MA, John C, Soler Artigas M, Bennett N, Hall R et al. Moderate-to-severe
922 asthma in individuals of European ancestry: a genome-wide association study. Lancet Respir
923 Med 2019; 7(1):20–34.
924 41. Marinho S, Custovic A, Marsden P, Smith JA, Simpson A. 17q12-21 variants are associated
925 with asthma and interact with active smoking in an adult population from the United Kingdom.
926 Ann Allergy Asthma Immunol 2012; 108(6):402-411.e9.
927 42. Hitomi Y, Kojima K, Kawashima M, Kawai Y, Nishida N, Aiba Y et al. Identification of the
928 functional variant driving ORMDL3 and GSDMB expression in human chromosome 17q12-21
929 in primary biliary cholangitis. Sci Rep 2017; 7(1):2904.
930 43. Keshari PK, Harbo HF, Myhr K-M, Aarseth JH, Bos SD, Berge T. Allelic imbalance of
931 multiple sclerosis susceptibility genes IKZF3 and IQGAP1 in human peripheral blood. BMC
932 Genet 2016; 17:59.
933 44. Quintana FJ, Jin H, Burns EJ, Nadeau M, Yeste A, Kumar D et al. Aiolos promotes TH17
934 differentiation by directly silencing Il2 expression. Nat Immunol 2012; 13(8):770–7.

935 45. Pfeffer PE, Hawrylowicz CM. Vitamin D in Asthma: Mechanisms of Action and
936 Considerations for Clinical Trials. Chest 2018; 153(5):1229–39.
937 46. Baeke F, Korf H, Overbergh L, van Etten E, Verstuyf A, Gysemans C et al. Human T
938 lymphocytes are direct targets of 1,25-dihydroxyvitamin D3 in the immune system. J Steroid
939 Biochem Mol Biol 2010; 121(1-2):221–7.
940 47. Zhu J, Cote-Sierra J, Guo L, Paul WE. Stat5 activation plays a critical role in Th2
941 differentiation. Immunity 2003; 19(5):739–48.

942

943 **Appendix 1**

944 **Primer sequences**

Gene	**species**	**sequence**
Gsdma antisense	mouse	5'-TCA ACC AGC TTC AGT TGC AC-3'
Gsdma sense	mouse	5'-TGC TGT CAA AGG ACG CTA TG-3'
Ikzf3 sense	mouse	5'-TGT CAC CTC TGC AAC TAC GC-3'
Ikzsf3 antisense	mouse	5'-TTC CGC AGA ACT CAC ACT TG-3'
IL-2 antisense	mouse	5'-ATC CTG GGG AGT TTC AGG TT-3'
IL-2 sense	mouse	5'-CCC ACT TCA AGC TCC ACT TC-3'
Ormdl3 antisense	mouse	5'-CTT TGC CTT GGT CTG GAG TC-3'
Ormdl3 sense	mouse	5'-CAC ACG GGT GAT GAA C AG TC-3'
Stat3 antisense	mouse	5'-TCG TGG TAA ACT GGA CAC CA-3'
Stat3 sense	mouse	5'-GAG GAG CTG CAG CAG AAA GT-3'
Stat5a antisense	mouse	5'-GTC AAA CTC GCC ATC TTG GT-3'

Stat5a sense	mouse	5'-TAC ATG GAC CAG GCT CCT TC-3'
Stat5b antisense	mouse	5'-TGG GTG GCC TTA ATG TTC TC-3'
Stat5b sense	mouse	5'-TGT GGA TAC AGG CTC AGC AG-3'

945

946

947 **Appendix 2**

948 **Antibodies**

Antibody	**clone**	**Vendor**	**catalog #**
Aiolos PE	8B2	Biolegend	653204
CD122 (IL2Rβ) APC	5H4	Biolegend	5H4
CD19 PE-Cy7	6D5	Biolegend	115520
CD4 FITC	RM4-5	Biolegend	100510
CD4 PerCPeFluor710	RM4-5	eBioscience	46-0042-82
CD44 FITC	IM7	Biolegend	103006
CD45 BV421	104	Biolegend	109832
CD62L PE	MEL-14	Biolegend	104408
CD8a APC-Cy7	53-6.7	Biolegend	100714
Foxp3 PE	FJK-16s	Invitrogen	12-5773-82
Gata3 PE	16E10A23	Biolegend	653804
IFNg FITC	XMG1.2	Biolegend	505806
IL-10 Pacific Blue	JES5-16E3	Biolegend	505020
IL-13 eFluor660	eBio13A	eBioscience	50-7133-82
IL-13 PE	eBio13A	molecular probes	A18492

IL17A PE-Cy7	TC11-18H10.1	Biolegend	506922
IL-2 PE-TexasRed	JES6-5H4	Biolegend	503840
monoclonal b-actin-Peroxidase	AC-15	Sigma-Aldrich	A3854
Phospho-BTK/ITK	M4G3LN	eBioscience	12-9015-42
Tbet PE	4B10	Biolegend	644809
VDR	D2K6W	Cell Signaling Technology	12550S
VDR AlexaFluor647	D2K6W	Cell Signaling Technology	custom order

949

950 **Appendix 3**

Reagent	**Vendor**	**catalog #**
anti-mouse CD28 (37.51)	BD Biosciences	553294
anti-mouse CD3e (145-2C11)	BD Biosciences	553057
b-mercaptoethanol	gibco	21985-032
calcitriol	Sigma-Aldrich	D1530
collagenase D	Roche	11088866001
Kwik-Diff soultion	Shandon	9990700
DMSO	Sigma-Aldrich	D2438
ProLong gold Anitfade Mountant with DAPI	ThermoFisher Scietific	P36935
rat anti-mouse anti-IFNg	BD Biosciences	554430
Anti-Mouse CD16/CD32 (Mouse BD Fc Block	BD Biosciences	553141
hamster anti-mouse anti-IL-4 (11B11)	BD Biosciences	554433
L-Glutamin	Sigma- Aldrich	G7513
LS columns	Miltenyi	130-042-401

microRNeasy	Qiagen	74004
naive CD4+ T cell isolation kit	Miltenyi	130-104-453
MEM non-essential amino acid solution (100x)	Sigma- Aldrich	M7145
Penicillin/Streptomycin	Sigma- Aldrich	P4333
Cell stimulation Cocktail (500x) phorbol myristate acetate (PMA)/Ionomycin	Tocris	TNB-4975
phosphate buffered saline	Gibco	14190-144
recombinant human TGFb1	Peprotech	100-21C
recombinant mouse IL-12	Peprotech	210-12
recombinant mouse IL-13	Peprotech	210-13
recombinant mouse IL-2	Peprotech	212-12
recombinant mouse IL-33	Peprotech	210-33
recombinant mouse IL-4	Peprotech	214-14
recombinant mouse IL-6	Peprotech	216-16
recombinant human IL-2	Peprotech	200-02
RPMI1640	Sigma-Aldrich	R8758
STAT3 inhibitor III WP1066	Sigma-Aldrich	573129
STAT5 inhibitor	EMD Millipore	573106
AS1517499 (STAT6 inhibitor)	Millipore-Sigma	SML190
U0126	CellSignaling Technologies	9903S
LY294002	CellSignaling Technologies	9901S

SsoFast Eva Green	Bio-Rad	1725201
10x zink fixative	BD Pharmingen	552658
Tris-Glycine-SDS Running Buffer	Boston Bioproducts	BP-150
Transfer buffer	Boston Bioproducts	BP-190
Tris Buffered Saline with Tween 20	CellSignaling Technologies	9997S

951

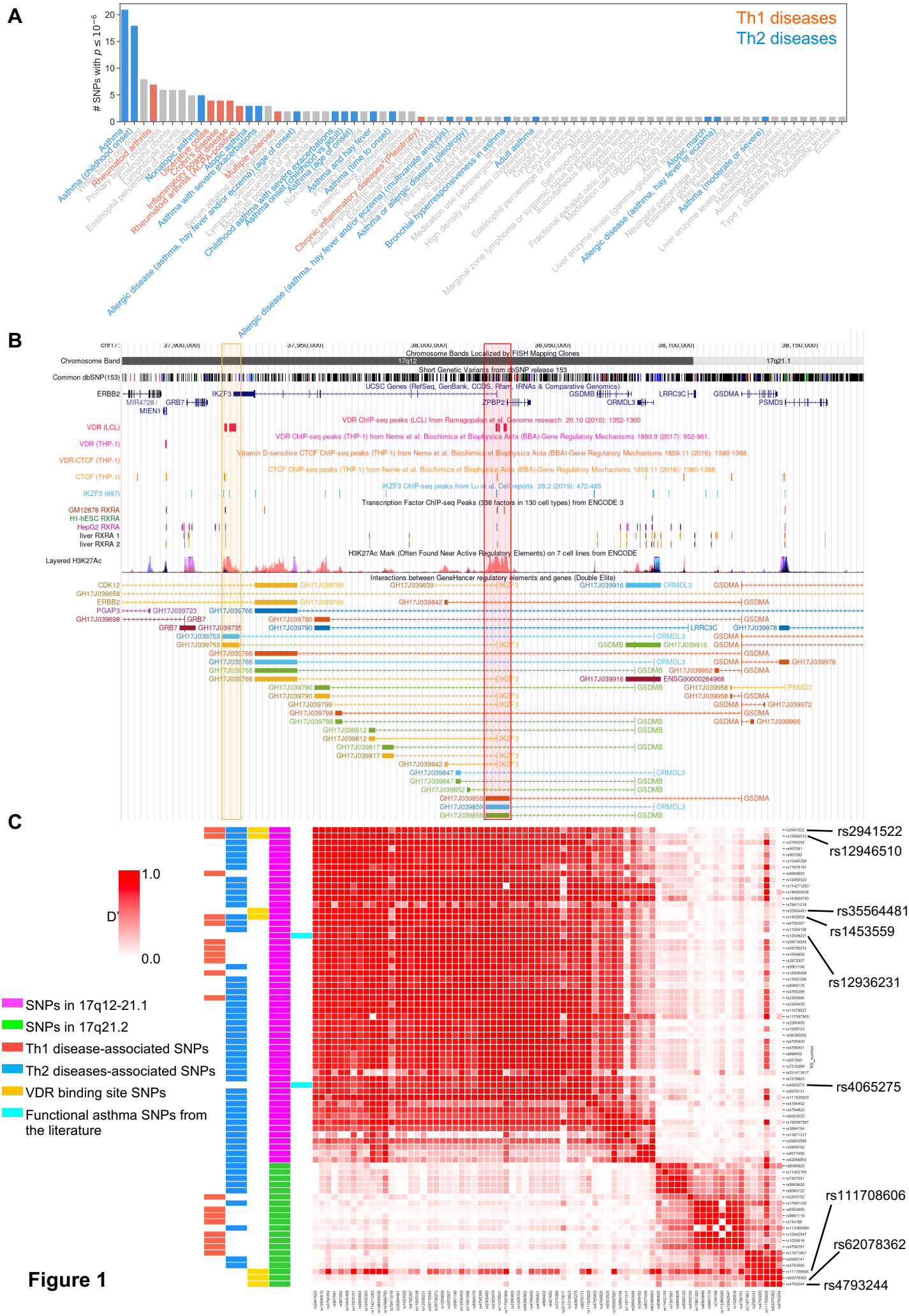
A
Th1 diseases
Th2 diseases
SNPs with p ≤ 10^-6
B
Chromosome Band
Common dbSNP(153)
UCSC Genes (RefSeq, GenBank, CCDS, Rfam, tRNAs & Comparative Genomics)
VDR (LCL)
VDR (THP-1)
VDR-CTCF (THP-1)
CTCF (THP-1)
IKZF3 (697)
Transcription Factor ChIP-seq Peaks (338 factors in 130 cell types) from ENCODE 3
Layered H3K27Ac
H3K27Ac Mark (Often Found Near Active Regulatory Elements) on 7 cell lines from ENCODE
Interactions between GeneHancer regulatory elements and genes (Double Elite)
C
D'
1.0
0.0
SNPs in 17q12-21.1
SNPs in 17q21.2
Th1 disease-associated SNPs
Th2 diseases-associated SNPs
VDR binding site SNPs
Functional asthma SNPs from the literature
rs2941522
rs12946510
rs35564481
rs1453559
rs12936231
rs4065275
rs111708606
rs62078362
rs4793244

Figure 1

A

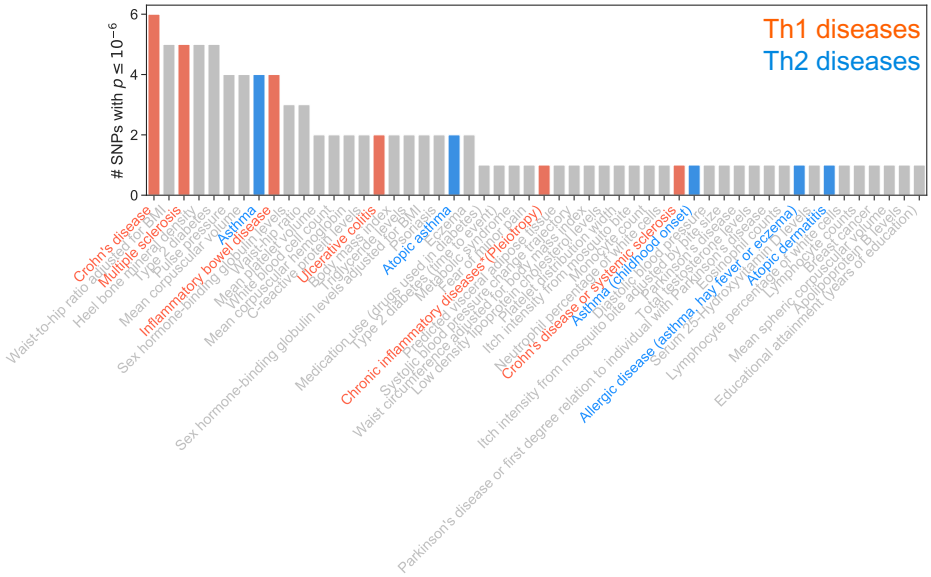

B

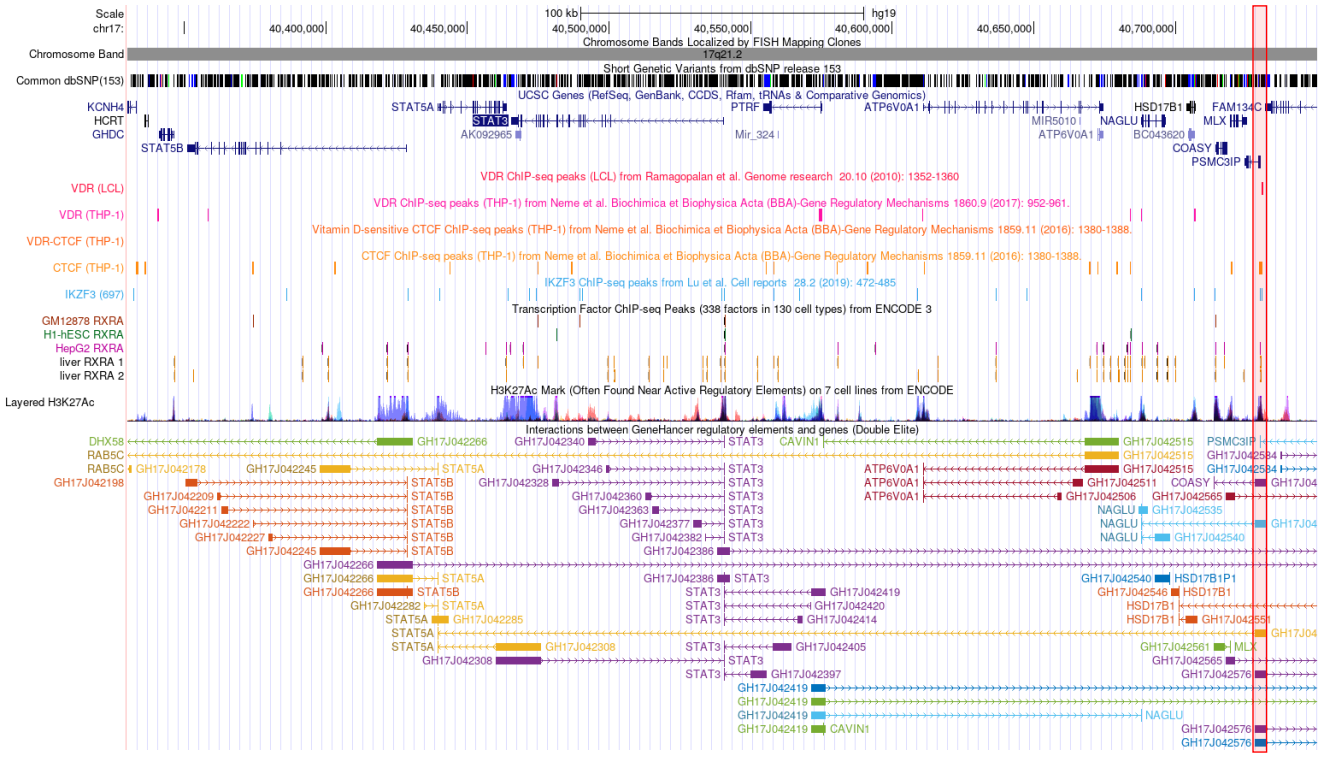

Figure 1-figure supplement 1

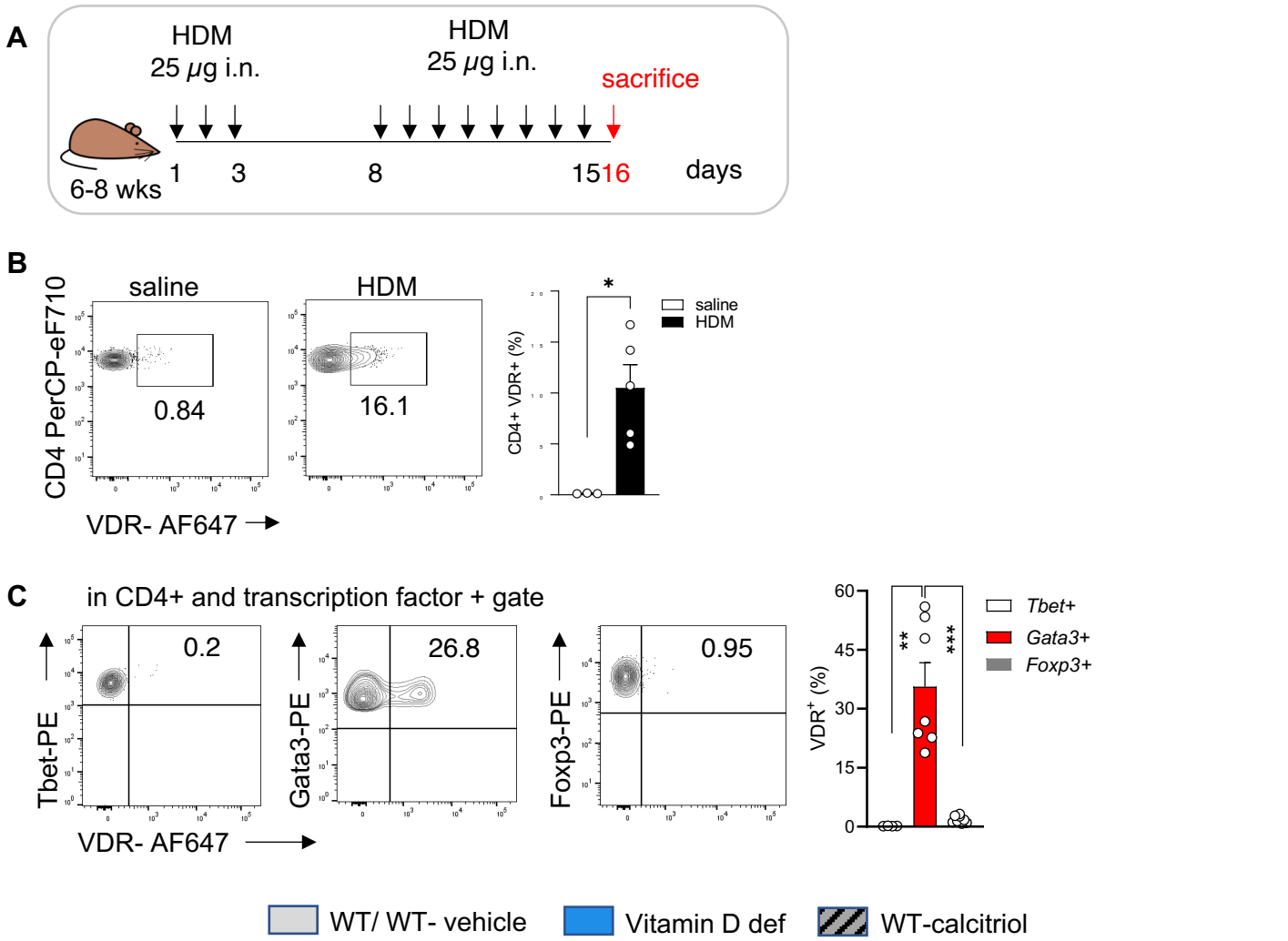
A
HDM
25 μg i.n.
HDM
25 μg i.n.
sacrifice
6-8 wks
1
3
8
15
16
days
B
saline
HDM
CD4 PerCP-eF710
0.84
16.1
VDR- AF647
CD4+ VDR+ (%)
saline
HDM
C
in CD4+ and transcription factor + gate
Tbet-PE
0.2
Gata3-PE
26.8
Foxp3-PE
0.95
VDR- AF647
VDR+ (%)
Tbet+
Gata3+
Foxp3+
WT/ WT- vehicle
Vitamin D def
WT-calcitriol
D
Ikzf3
Ormdl3
Gsdma
rel. mRNA expression
f
E
Stat5a
Stat5b
Stat3
ns
g

Figure 2

A gating strategy

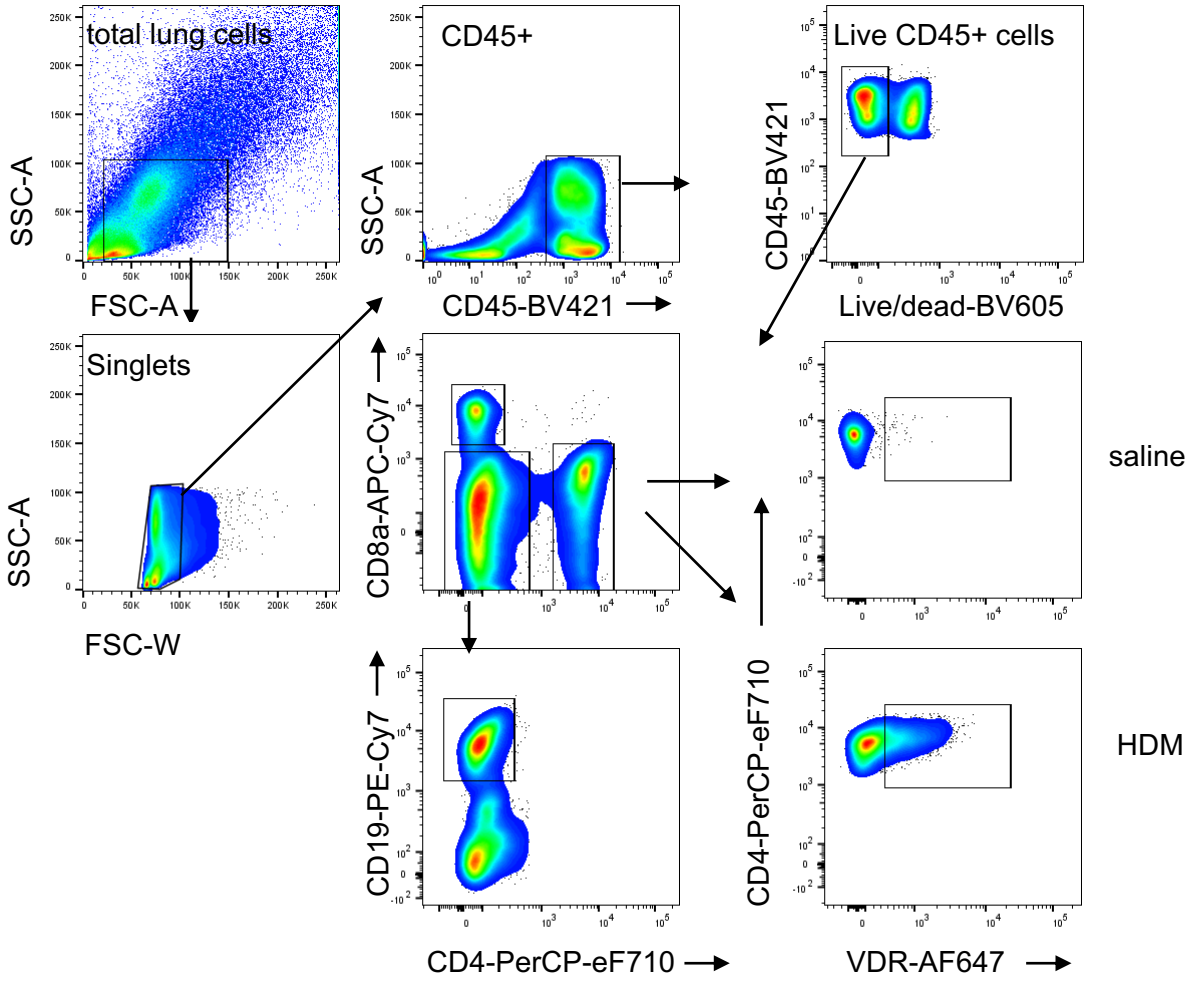

B

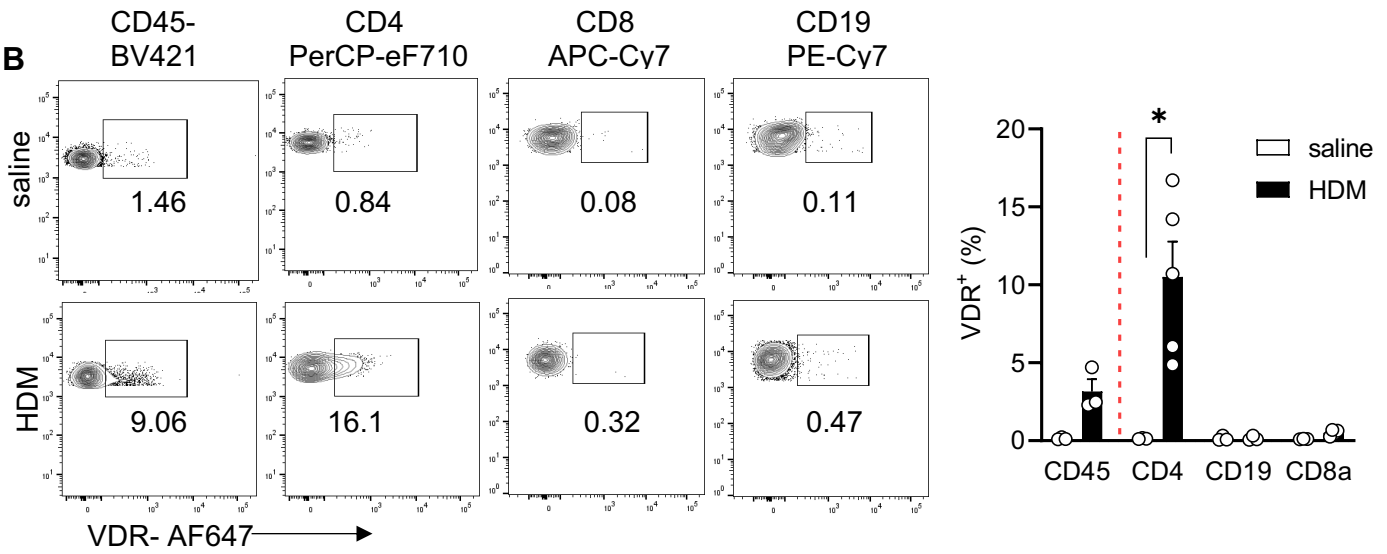

C gated on CD45+ CD4+

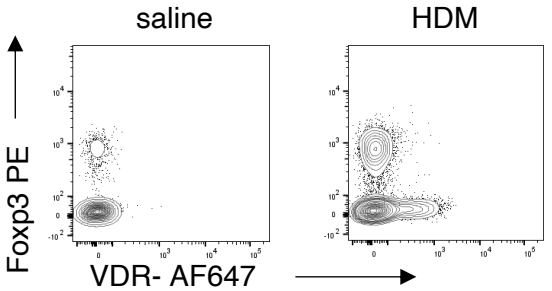

Figure 2 - figure supplement 1

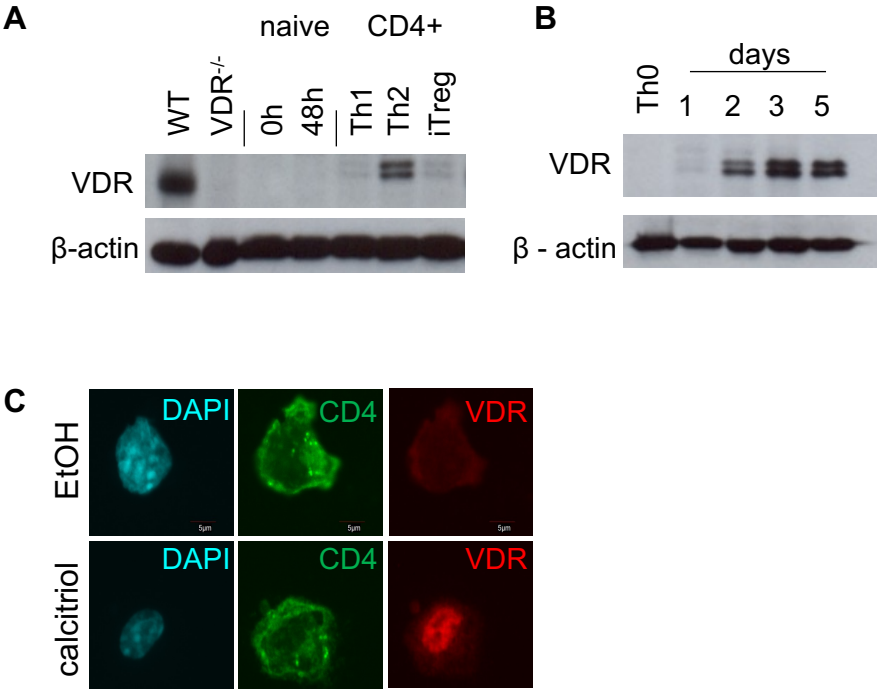

Figure 2 - figure supplement 2

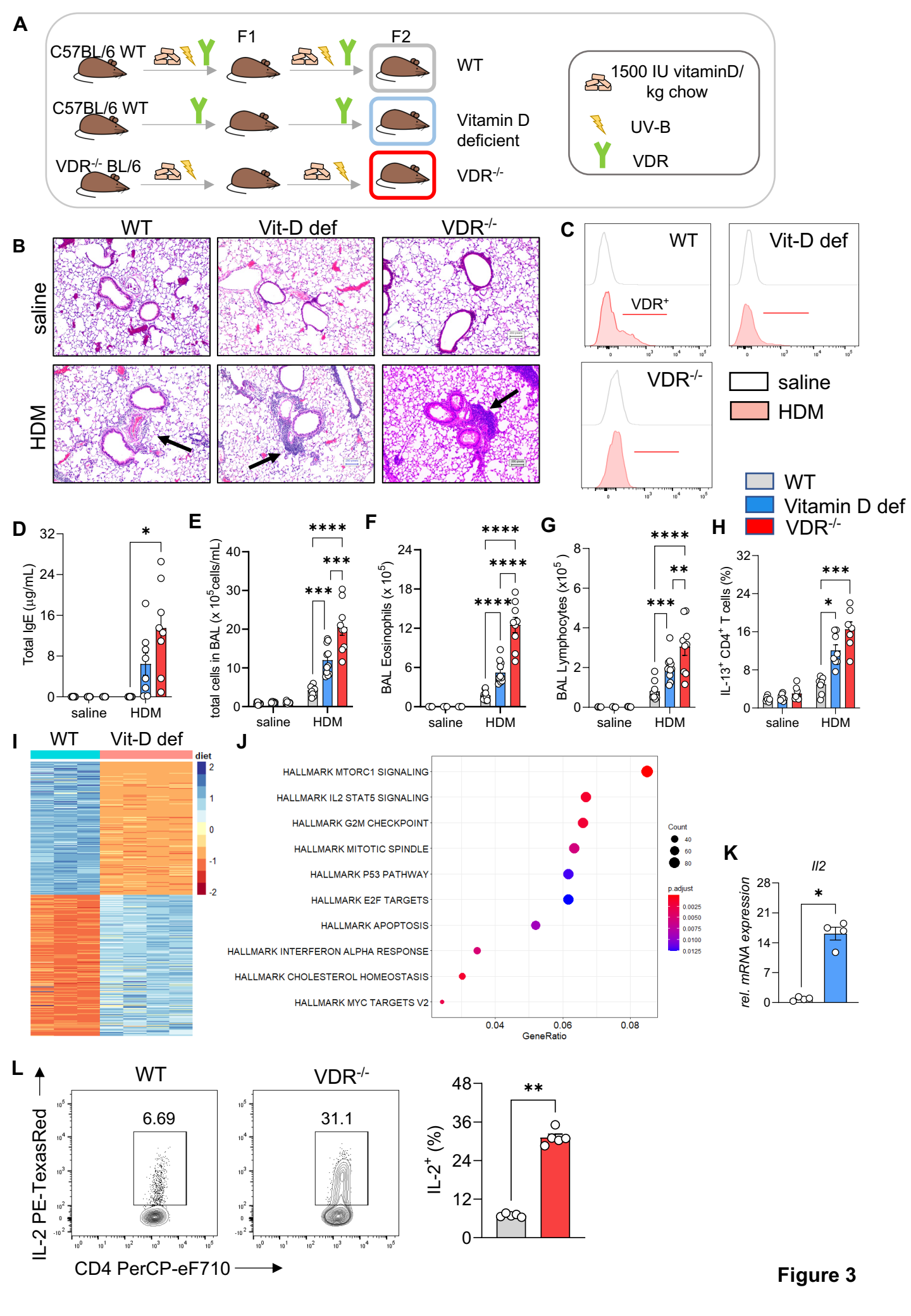
A
C57BL/6 WT
F1
F2
WT
C57BL/6 WT
Vitamin D deficient
VDR-/- BL/6
VDR-/-
1500 IU vitaminD/ kg chow
UV-B
VDR
B
WT
Vit-D def
VDR-/-
saline
HDM
C
WT
Vit-D def
VDR+
VDR-/-
saline
HDM
WT
Vitamin D def
VDR-/-
D
Total IgE (µg/mL)
saline
HDM
E
total cells in BAL (x 10^5 cells/mL)
F
BAL Eosinophils (x 10^5)
G
BAL Lymphocytes (x10^5)
H
IL-13+ CD4+ T cells (%)
I
WT
Vit-D def
diet
J
HALLMARK MTORC1 SIGNALING
HALLMARK IL2 STAT5 SIGNALING
HALLMARK G2M CHECKPOINT
HALLMARK MITOTIC SPINDLE
HALLMARK P53 PATHWAY
HALLMARK E2F TARGETS
HALLMARK APOPTOSIS
HALLMARK INTERFERON ALPHA RESPONSE
HALLMARK CHOLESTEROL HOMEOSTASIS
HALLMARK MYC TARGETS V2
GeneRatio
Count
p.adjust
K
Il2
rel. mRNA expression
L
WT
VDR-/-
6.69
31.1
IL-2 PE-TexasRed
CD4 PerCP-eF710
IL-2+ (%)

Figure 3

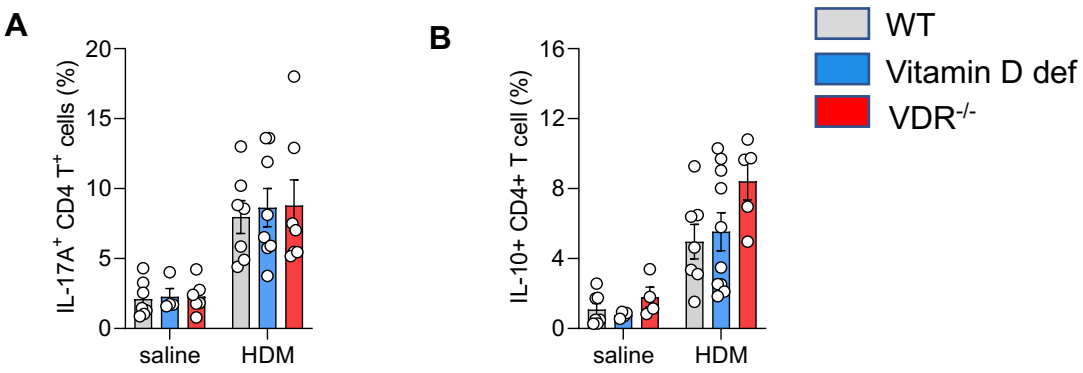

Figure 3 - figure supplement 1

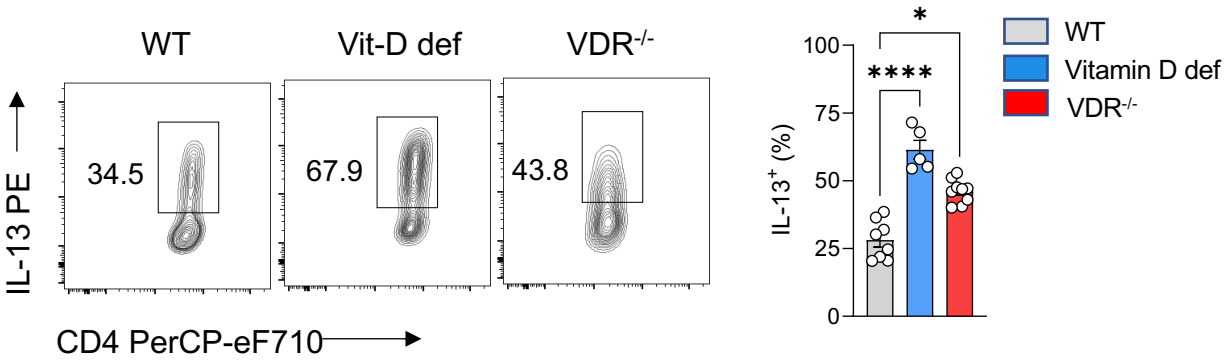

Figure 3 - figure supplement 2

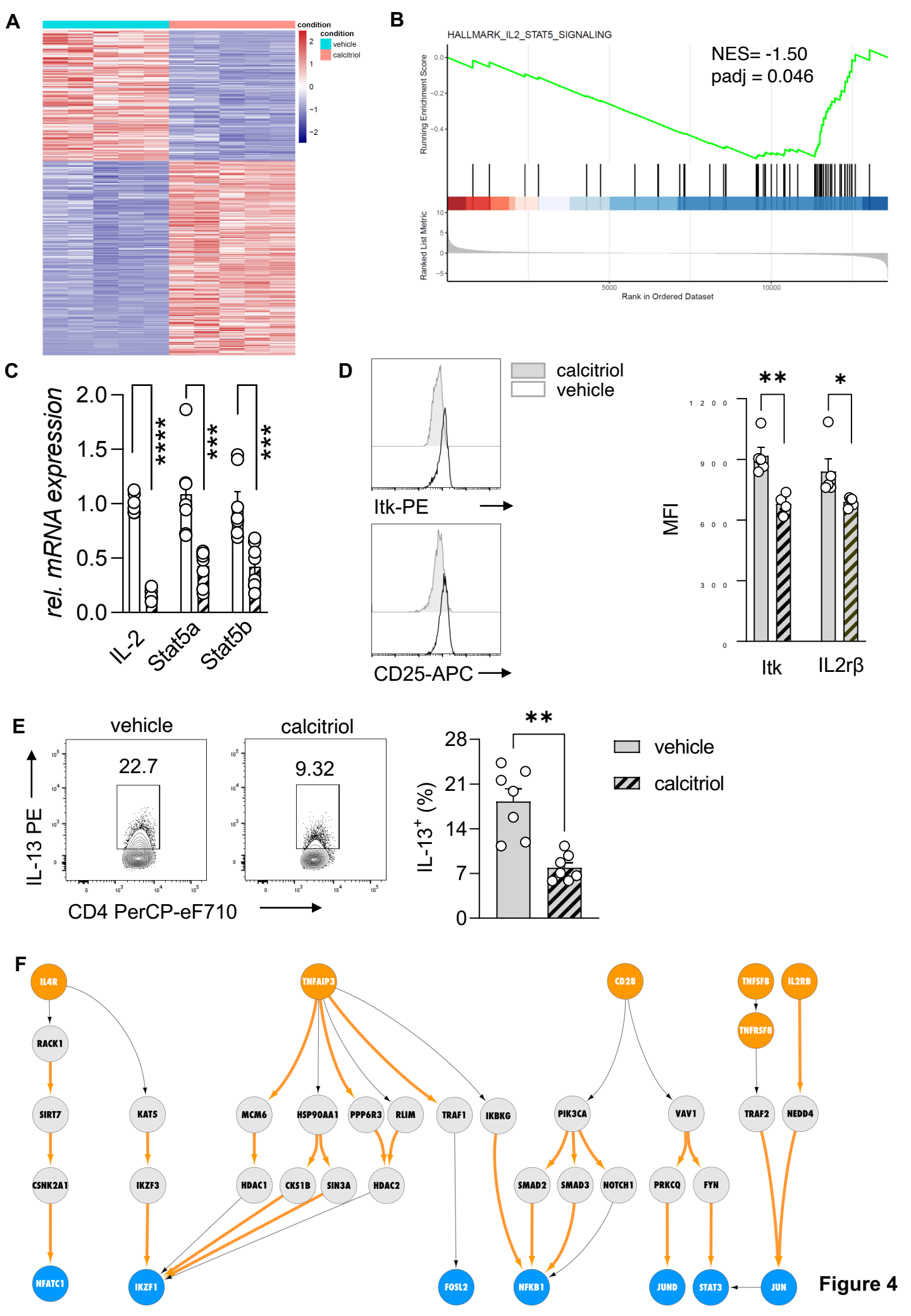
A
condition
vehicle
calcitriol
B
HALLMARK_IL2_STAT5_SIGNALING
NES= -1.50
padj = 0.046
Running Enrichment Score
Ranked List Metric
Rank in Ordered Dataset
C
rel. mRNA expression
IL-2
Stat5a
Stat5b
D
calcitriol
vehicle
Itk-PE
CD25-APC
MFI
Itk
IL2rβ
E
vehicle
calcitriol
22.7
9.32
IL-13 PE
CD4 PerCP-eF710
IL-13+ (%)
F
IL4R
RACK1
SIRT7
CSNK2A1
NFATC1
KAT5
IKZF3
IKZF1
TNFAIP3
MCM6
HSP90AA1
PPP6R3
RLIM
TRAF1
IKBKG
HDAC1
CKS1B
SIN3A
HDAC2
FOSL2
NFKB1
CD28
PIK3CA
SMAD2
SMAD3
NOTCH1
VAV1
PRKCQ
FYN
JUND
STAT3
TNFSF8
IL2RB
TNFRSF8
TRAF2
NEDD4
JUN

Figure 4

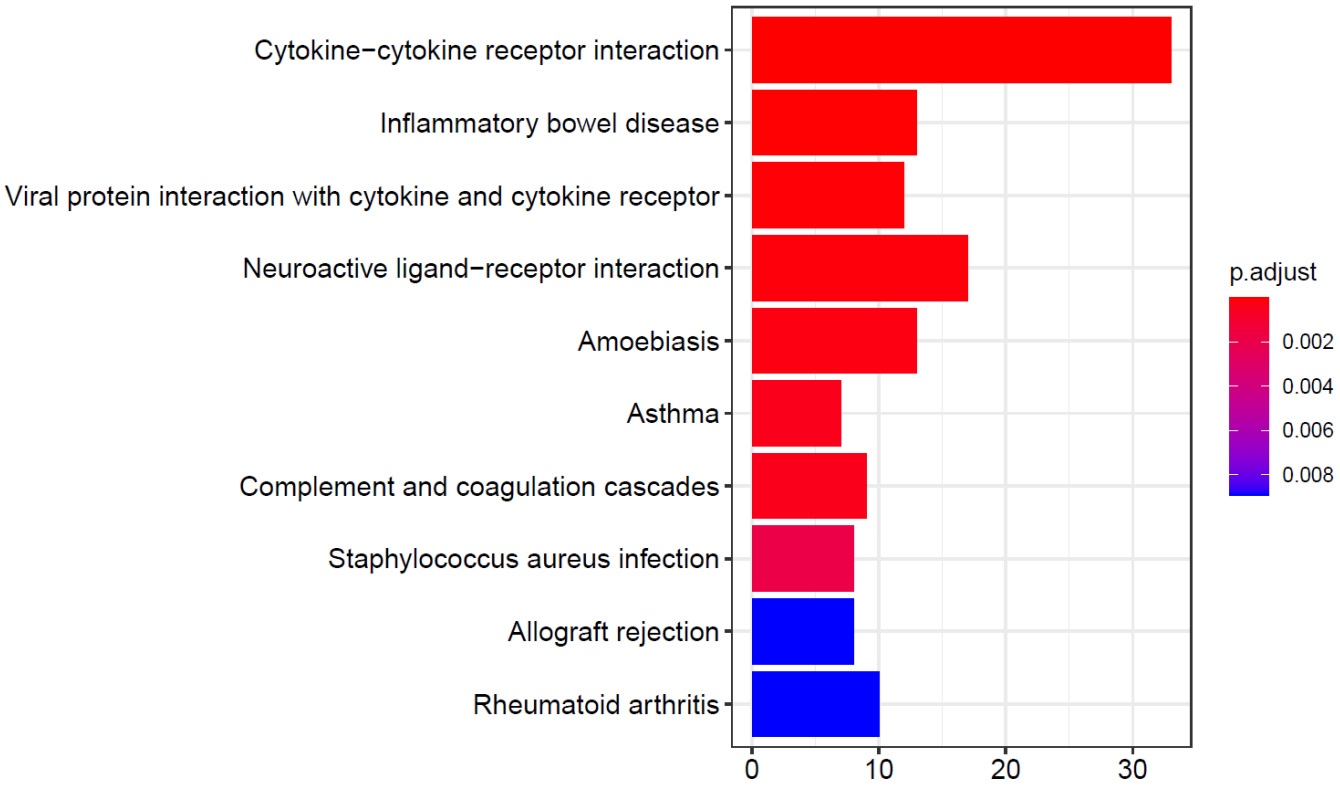

Figure 4 - figure supplement 1

A

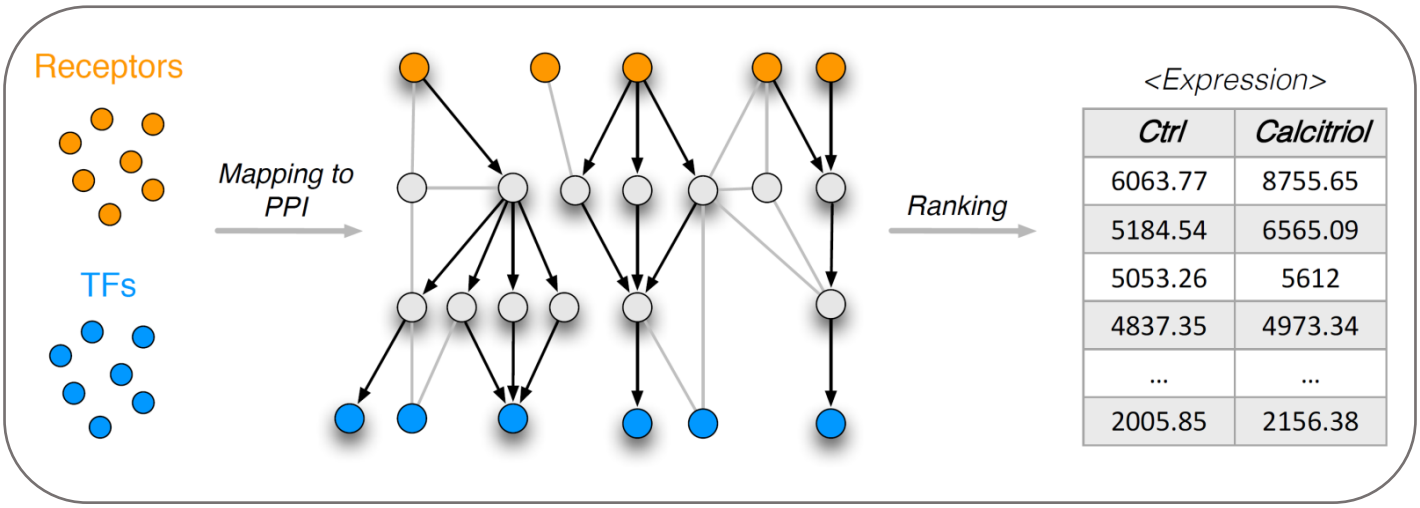

B

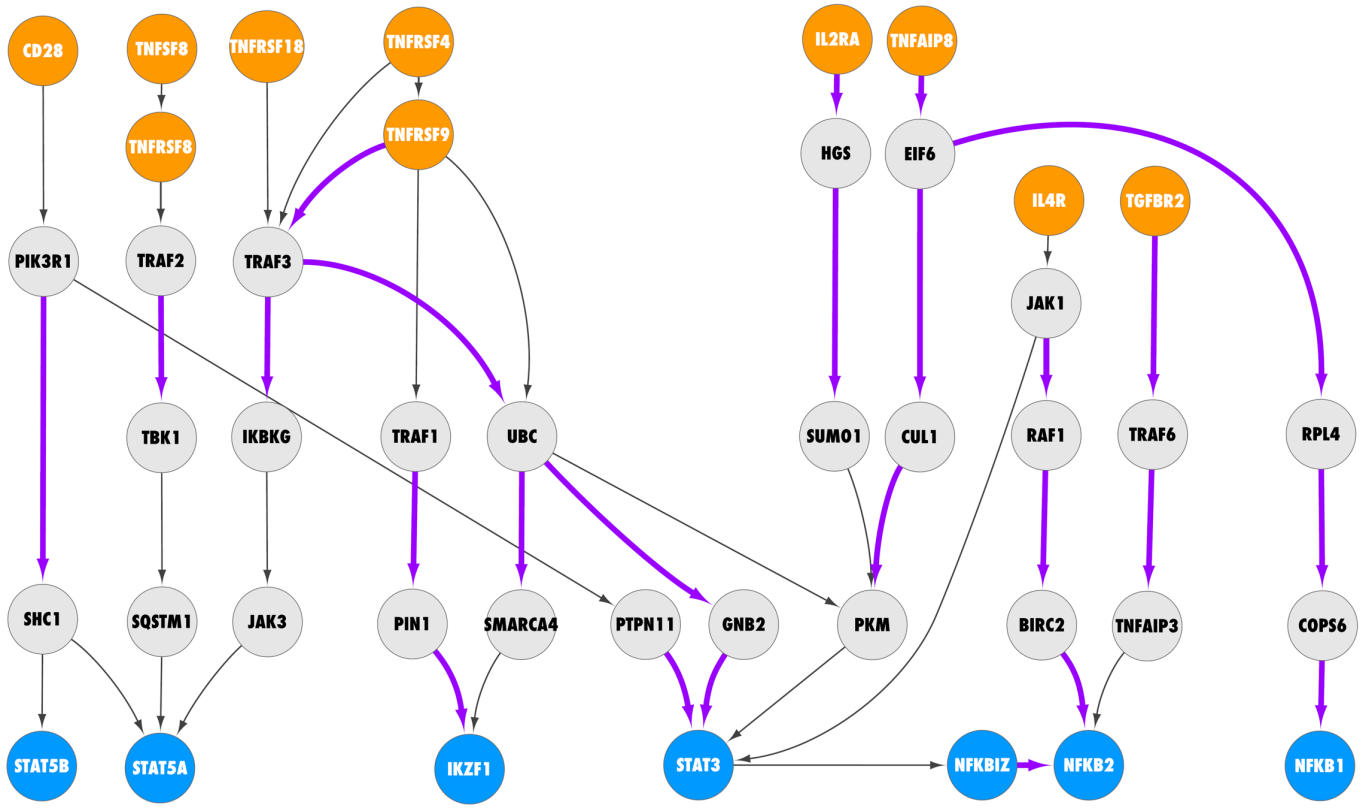

Figure 4 - figure supplement 2

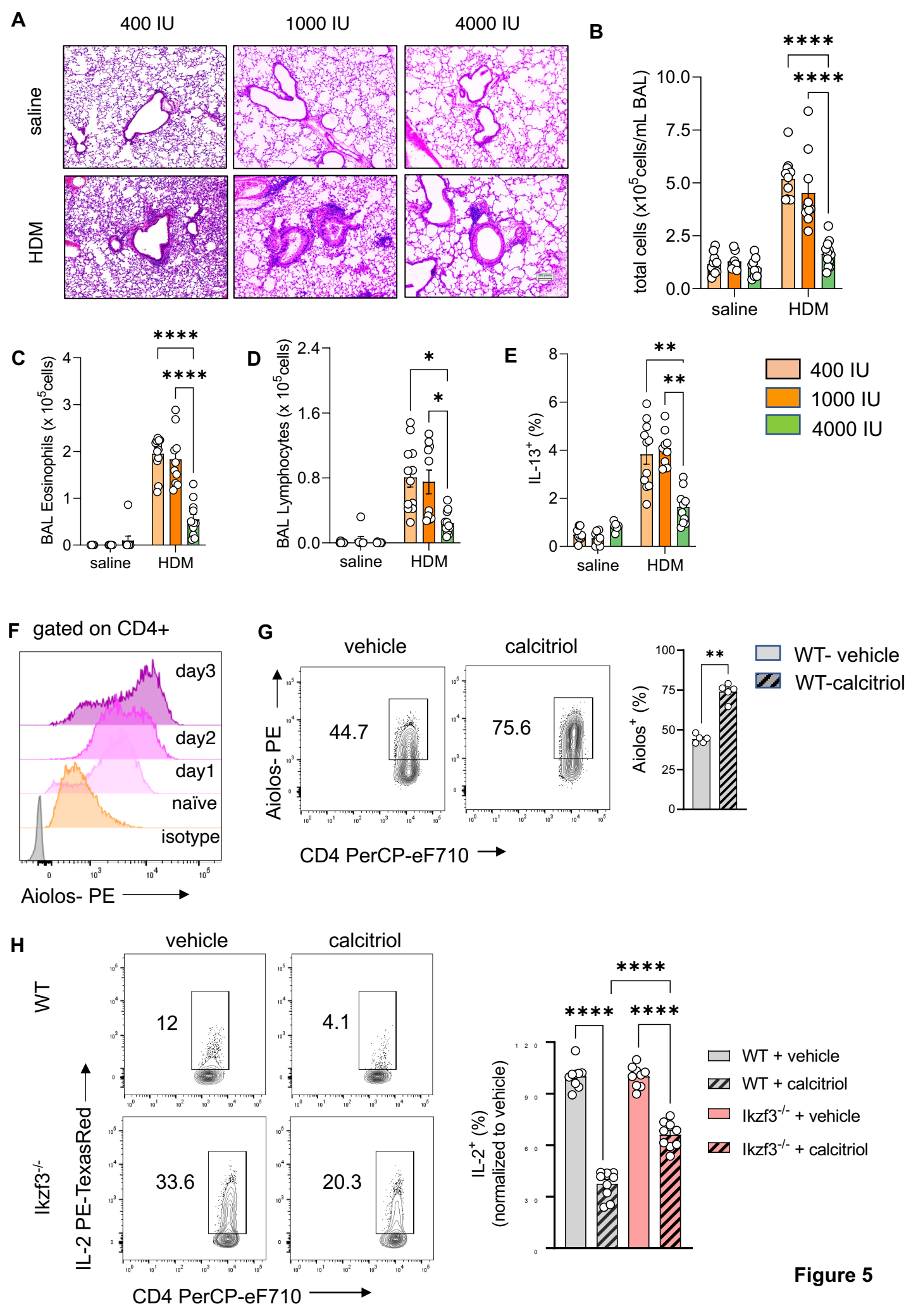
A
400 IU
1000 IU
4000 IU
saline
HDM
B
total cells (x10^5 cells/mL BAL)
10.0
7.5
5.0
2.5
0.0
saline
HDM
****
****
C
BAL Eosinophils (x 10^5 cells)
4
3
2
1
0
saline
HDM
****
****
D
BAL Lymphocytes (x 10^5 cells)
2.4
1.6
0.8
0.0
saline
HDM
*
*
E
IL-13+ (%)
8
6
4
2
0
saline
HDM
**
**
400 IU
1000 IU
4000 IU
F gated on CD4+
day3
day2
day1
naïve
isotype
Aiolos- PE
G
vehicle
calcitriol
44.7
75.6
Aiolos- PE
CD4 PerCP-eF710
Aiolos+ (%)
100
75
50
25
0
**
WT- vehicle
WT-calcitriol
H
vehicle
calcitriol
WT
Ikzf3-/-
12
4.1
33.6
20.3
IL-2 PE-TexasRed
CD4 PerCP-eF710
IL-2+ (%)
(normalized to vehicle)
****
****
****
WT + vehicle
WT + calcitriol
Ikzf3-/- + vehicle
Ikzf3-/- + calcitriol

Figure 5

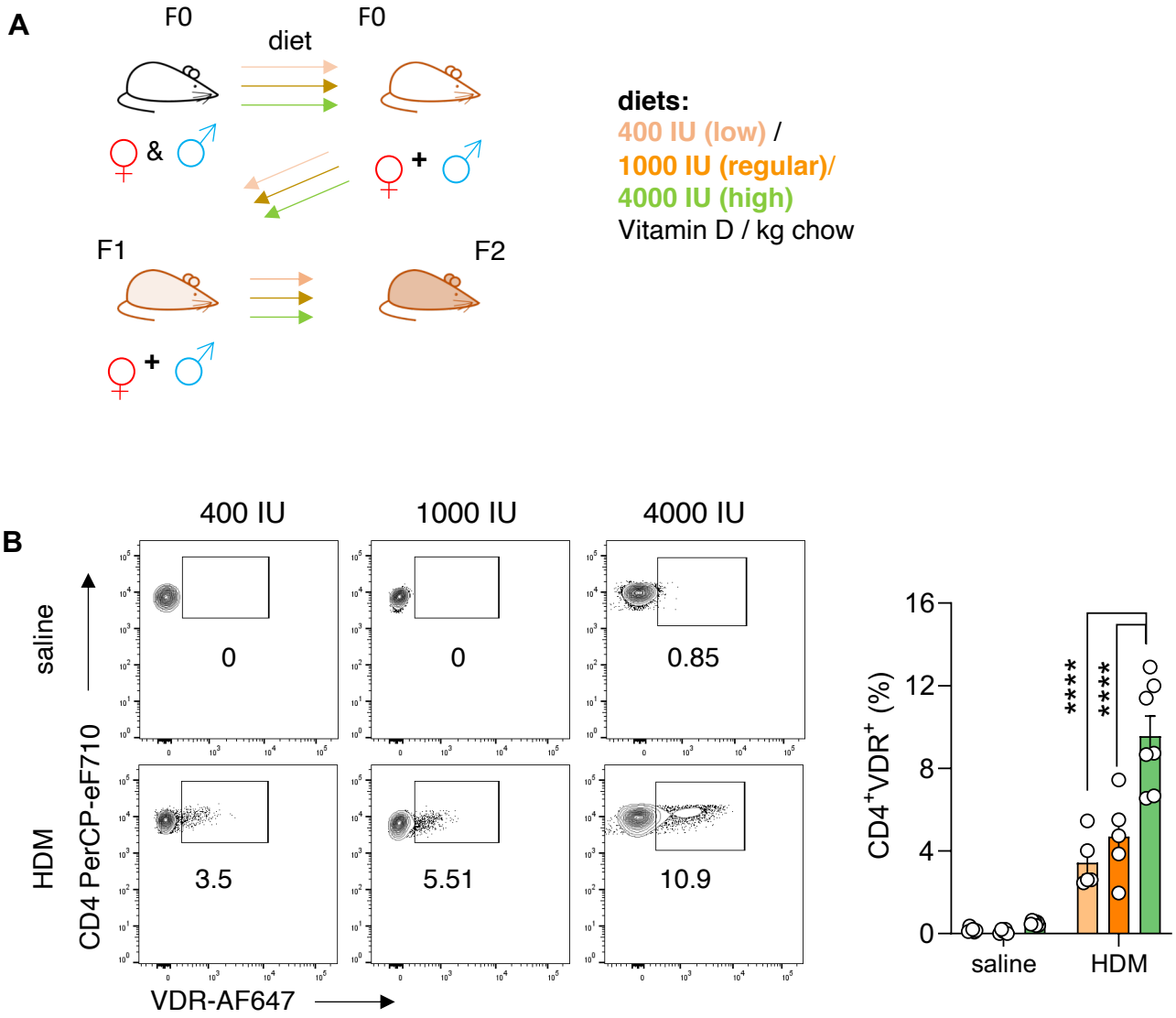

Figure 5 - figure supplement 1

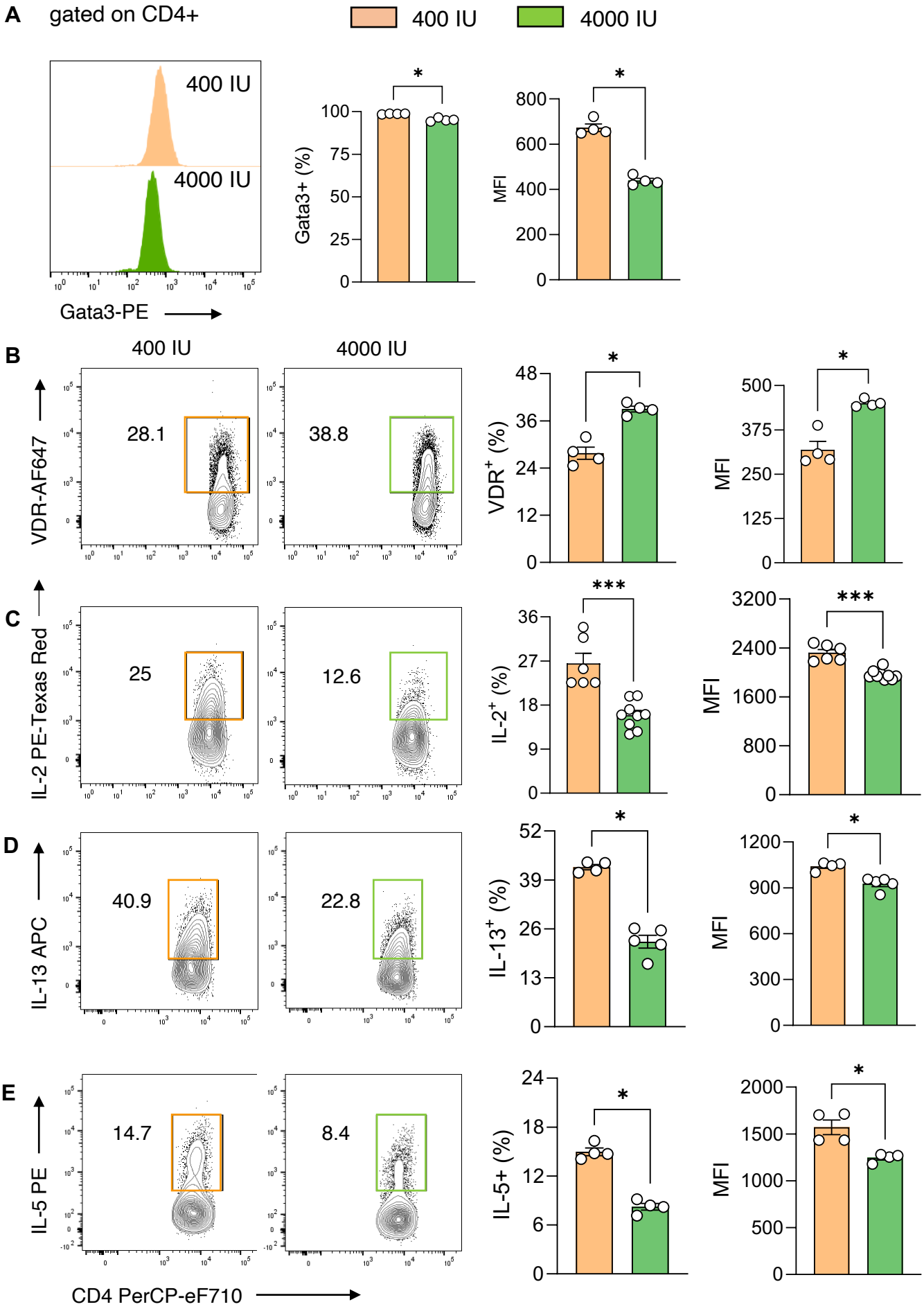

Figure 5 - figure supplement 2

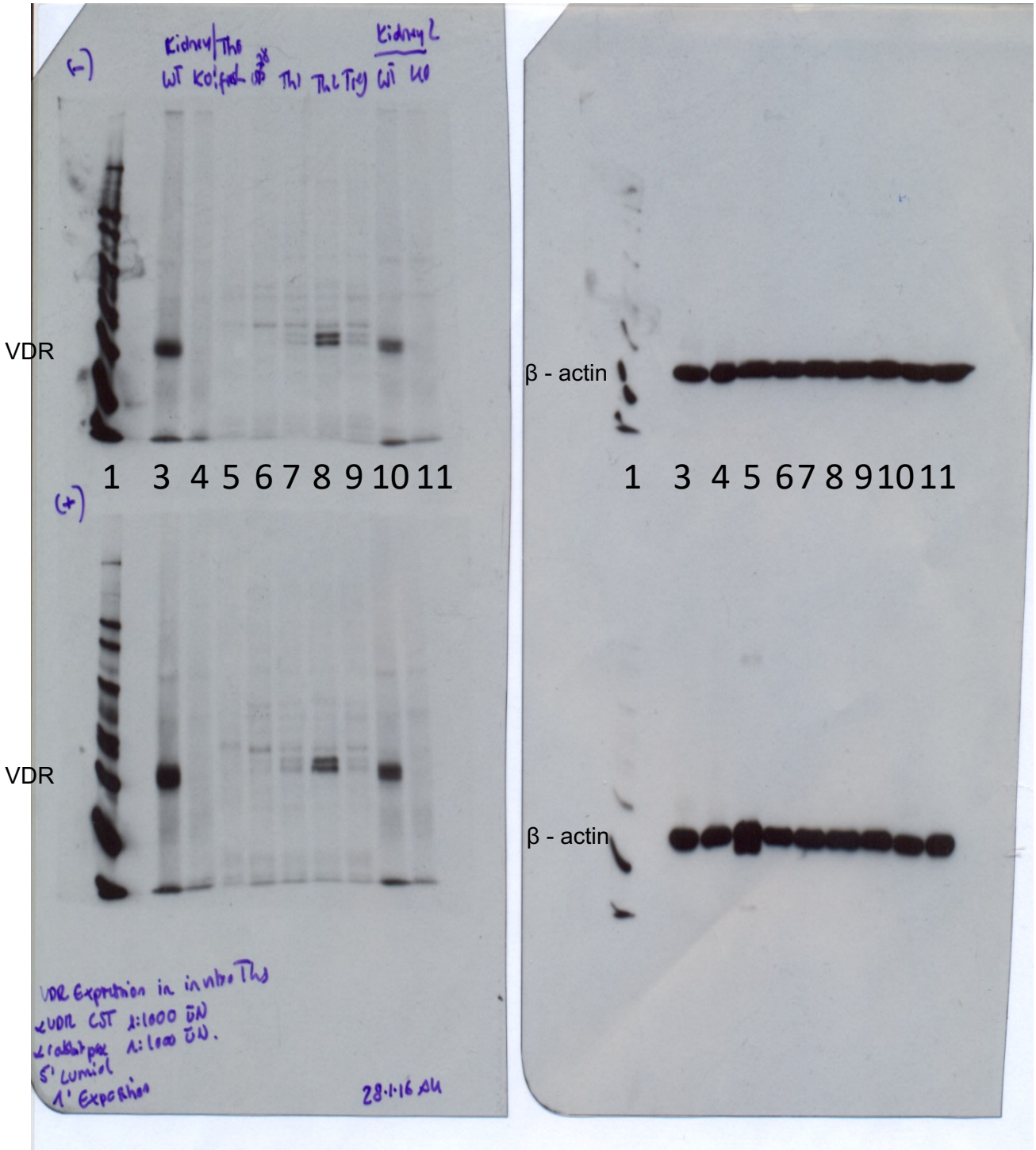

Loading order:
1- marker
2- empty
3- WT kidney sample: positive control
4- VDR-/- kidney sample: negative control
5- CD4+ CD62L+CD44- naïve T cells fresh
6- Th0 cells (24 h CD3 & CD28 stimulation)
7- in vitro Th1
8- in vitro Th2
9- in vitro iTreg
10- WT kidney sample: positive control
11- VDR-/- kidney sample: negative control

Source data-Figure 2 - figure supplement 2A

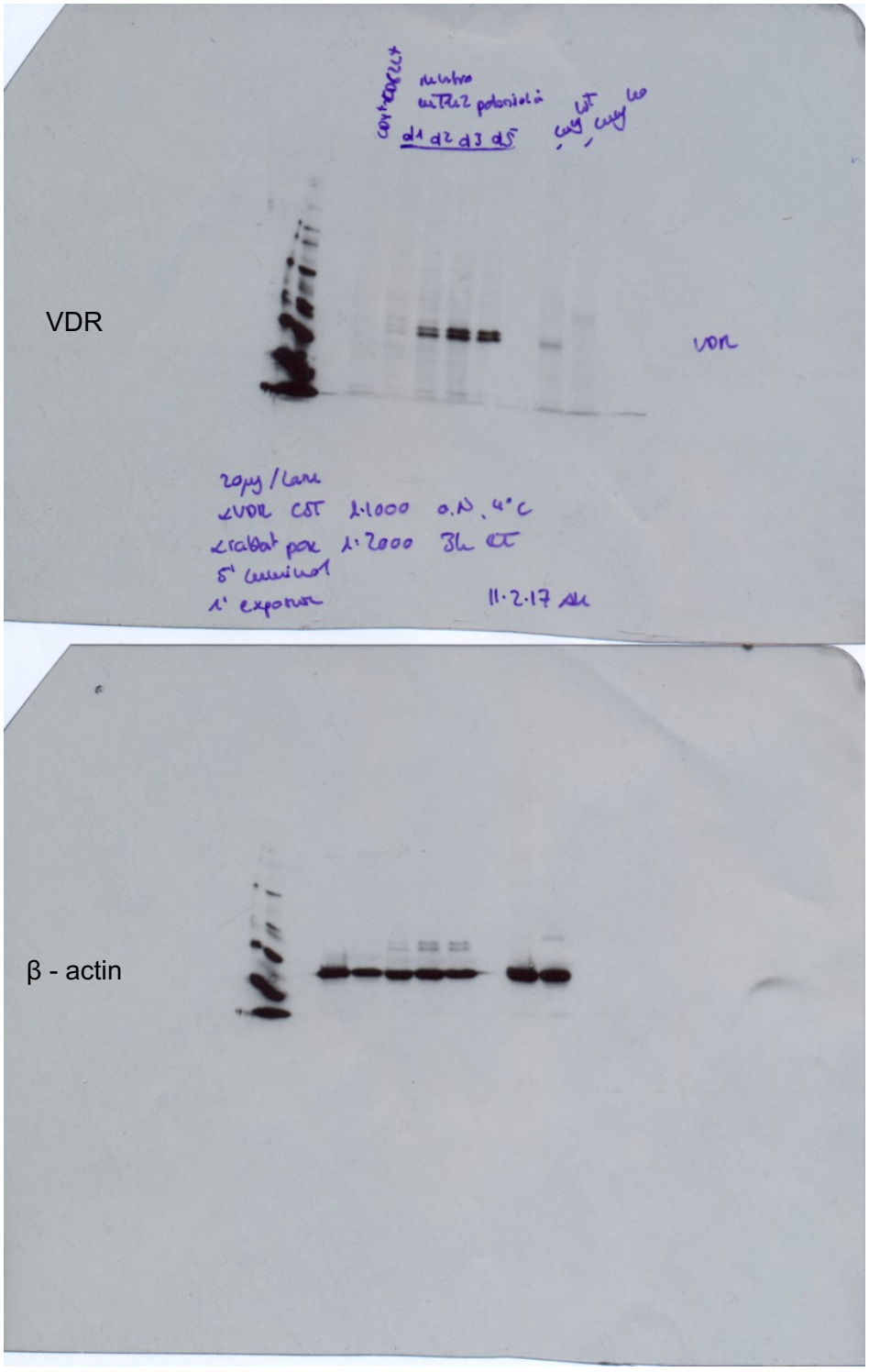

Loading order:
1- marker
2- empty
3- CD4+ CD62L+CD44- naïve T cells fresh
4- in vitro differentiating Th2 day 1
5- in vitro differentiating Th2 day 2
6- in vitro differentiating Th2 day 3
7- in vitro differentiating Th2 day 5
8- empty
9- WT lung sample: positive control
10- VDR-/- lung sample: negative control

Source data-Figure 2 - figure supplement 2B